arXiv:1409.6762v1 [astro-ph.SR] 23 Sep 2014

DRAFT: September 25, 2014

Outflows, Dusty Cores, and a Burst of Star Formation in the North America and Pelican Nebulae

John Bally[1,7], Adam Ginsburg[2], Ron Probst[3,7], Bo Reipurth[4],
Yancy L. Shirley[5], and Guy S. Stringfellow[6,7]

[1] *Department of Astrophysical and Planetary Sciences, University of Colorado, UCB 389, Boulder, CO 80309*

John.Bally@colorado.edu

[2] *European Southern Observatory, Karl-Schwarzschild-Str. 2, 85748 Garching bei Munchen, Germany*

aginsburg@eso.org

[3] *National Optical Astronomy Observatory, 950 North Cherry Avenue, Tucson, AZ 85719*

probst@noao.edu

[4] *Institute for Astronomy, University of Hawaii at Manoa, 640 N. A'ohoku Place, Hilo, HI 96720*

reipurth@ifa.hawaii.edu

[5] *Steward Observatory, University of Arizona, 933 North Cherry Ave., Tucson, AZ, 85721*

yshirley@as.arizona.edu

[6] *Center for Astrophysics and Space Astronomy, University of Colorado, UCB 389, Boulder, CO 80309*

Guy.Stringfellow@colorado.edu

[7] Visiting Astronomer, Kitt Peal National Observatory, National Optical Astronomy Observatories, which is operated by the Association of Universities for Research in Astronomy (AURA), Inc. under cooperative agreement with the National Science Foundation.

ABSTRACT

We present observations of near-infrared 2.12 μm molecular hydrogen outflows emerging from 1.1 mm dust continuum clumps in the North America and Pelican Nebula (NAP) complex selected from the Bolocam Galactic Plane Survey (BGPS). Hundreds of individual shocks powered by over 50 outflows from young stars are identified, indicating that the dusty molecular clumps surrounding the NGC 7000 / IC 5070 / W80 HII region are among the most active sites of on-going star formation in the Solar vicinity. A spectacular X-shaped outflow, MHO 3400, emerges from a young star system embedded in a dense clump more than a parsec from the ionization front associated with the Pelican Nebula (IC 5070). Suspected to be a binary, the source drives a pair of outflows with orientations differing by 80°. Each flow exhibits S-shaped symmetry and multiple shocks indicating a pulsed and precessing jet. The 'Gulf of Mexico' located south of the North America Nebula (NGC 7000), contains a dense cluster of molecular hydrogen objects (MHOs), Herbig-Haro (HH) objects, and over 300 YSOs, indicating a recent burst of star formation. The largest outflow detected thus far in the North America and Pelican Nebula complex, the 1.6 parsec long MHO 3417 flow, emerges from a 500 $M_\odot$ BGPS clump and may be powered by a forming massive star. Several prominent outflows such as MHO 3427 appear to be powered by highly embedded YSOs only visible at $\lambda > 70$ μm. An 'activity index' formed by dividing the number of shocks by the mass of the cloud containing their source stars is used to estimate the relative evolutionary states of Bolocam clumps. Outflows can be used as indicators of the evolutionary state of clumps detected in mm and sub-mm dust continuum surveys.

Subject headings: ISM: Herbig-Haro objects – ISM: individual (NGC 7000, IC5070, LDN 935) – ISM: jets and outflows – stars: formation

1. Introduction

Recent millimeter and sub-millimeter wavelength surveys of the Galactic plane have found many thousands of dense, dusty clumps embedded within molecular clouds, many of which are destined to form groups, associations, or clusters of stars. The Bolocam Galactic Plane Survey (BGPS) used the Caltech Sub-millimeter Observatory (CSO) to survey the northern Galactic plane at a wavelength of 1.1 mm with an angular resolution $\sim 33''$,

finding about 10^4 clumps with masses ranging from a few to over 10^4 $M_\odot$ (Aguirre et al. 2011; Ginsburg et al. 2013) . A key observational challenge is to determine the evolutionary state of dense, self-gravitating clumps to determine which ones are pre-stellar, or actively forming stars, or near the end of star-formation and in the process of being disrupted.

The amount of star formation, and hence the evolutionary state of a clump, can be estimated from its content of young stellar objects (YSOs). Embedded YSOs can be identified by their infrared excess emission or protostellar outflows. In this study, we investigate the distribution of protostellar outflows as traced by near infrared (NIR) emission in the 1.644 μm [Fe II] and 2.122 μm H_2 lines which trace shocks in lightly-obscured (A_V less than about 15 magnitudes) molecular gas in the North America and Pelican Nebulae. Shocks detected in visual-wavelength Hα and [S II] emission (Herbig-Haro objects) which can be seen when A_V is less than a few magnitudes and *Spitzer* Space Telescope detections of YSOs are combined with our data to trace recent and on-going star formation in these clumps.

The North America and Pelican (hereafter NAP) Nebulae (NGC 7000 and IC 5070) are parts of a single, 3° diameter HII region in Cygnus called W80 which is located at the high-Galactic-longitude side of the Cygnus-X complex of star formation regions in a spiral arc or spur in our Galaxy (Reipurth & Schneider 2008; Guieu et al. 2009). The distance to this complex has been estimated to be between 500 pc to over 1 kpc (Reipurth & Schneider 2008). A distance of 550 pc is adopted here for the NAP complex (Laugalys et al. 2006), making the NAP one of the nearest regions that formed massive stars in the recent past.

W80 is a mature HII region which has swept-up and accelerated considerable amount of molecular gas (Bally & Scoville 1980) and the molecular clouds at its periphery exhibit on-going star formation activity. The two nebulae, NGC 7000 and IC 5070, are separated by a large dust cloud called L935. The highly opaque southern portion of L935 resembles the 'Gulf of Mexico' (hereafter Gulf) while the less opaque central portion looks like the 'Atlantic Ocean', giving the North America Nebula its name (Figure 1). L935 is the foreground part of a giant molecular cloud associated with W80. Molecular clouds associated with the NAP have a total mass of about 3×10^4 $M_\odot$ (Bally & Scoville 1980) to 5×10^4 $M_\odot$ (Feldt & Wendker 1993). The North America and Pelican Nebulae each contain an association of T Tauri stars (Herbig & Bell 1988). The clouds northwest of the Pelican and those in the 'Gulf' region each contain a large number of protostellar outflows traced by visual-wavelength shocks - Herbig-Haro Objects - (Bally & Reipurth 2003; Armond et al. 2011).

The radial velocity field in CO indicates that the expansion of the W80 HII region may have swept-up, compressed, and accelerated the clouds surrounding W80, resulting in 3 to 5 km s^{-1} blueshift of L935 (the 'Gulf' and the 'Atlantic Ocean') with respect to the clouds lying along the projected edge of the HII region (Bally & Scoville 1980). Most of

the massive stars responsible for ionization of W80 are hidden behind L935. Straižys & Laugalys (2008) identified a number of candidate massive stars in this region. In particular, their star #7 (2MASS J20552516+4418144), located behind the northeastern edge of the "Atlantic Ocean", and #8 (the Comerón & Pasquali star; 2MASS J20555125+4352246), located northwest of the 'Gulf' have spectral types O5V (Comerón & Pasquali 2005).

The molecular clouds associated with the W80 complex contain several dozen dense dust clumps recently mapped at a wavelength of 1.1 mm by the BGPS described in Aguirre et al. (2011), Rosolowsky et al. (2010), and Ginsburg et al. (2013). The Gulf of Mexico is seen as an infrared dark cloud (IRDC) against the background emission at wavelengths between 3.6 and 24 μm. This cloud, G084.81–01.09, is associated with the largest and brightest 1.1 mm clumps in the NAP and has been mapped recently in several transitions of NH_3, ^{12}CO, ^{13}CO, $C^{18}O$, and HCO^+, providing measurements of central velocities, line-widths, densities, and gas temperatures (Zhang et al. 2011). These authors found six ammonia clumps with masses ranging from 60 to 250 $M_\odot$, gas temperatures of order 12 K, and molecular hydrogen densities of order $n(H_2) \sim 10^5$ cm^{-3}. Guieu et al. (2009) presented *Spitzer* Space Telescope IRAC observations and Rebull et al. (2011) used *Spitzer* MIPS data to identify about 2,000 candidate YSOs in the NAP of which over 300 are concentrated in the Gulf. Thus, the NAP contains one of the largest concentrations of YSOs in the Solar vicinity.

The observations discussed here are described in Section 2. The observational results are described in Section 3 starting with the Pelican region (Section 3.1), the Atlantic region (Section 3.2), and the Gulf of Mexico region (Section 3.3). Section 4 discusses the properties of the BGPS clumps and a group of small cometary clouds seen in the IR images. Section 5 presents a discussion of the results. Subsection 5.1 discusses the evolutionary states of the NAP clumps, subsection 5.2 looks at triggering, and subsection 5.3 reviews the star formation efficiency in the NAP. Section 6 presents the conclusions.

2. Observations

In this paper, near-infrared, narrow-band images of 2.122 μm emission from shock-excited and fluorescent H_2 are presented. The dominant physical mechanisms in our sources are inferred from morphology, association with optical emission lines, and comparison to other sources studied with spectroscopy. For example, in the Orion Nebula region, spectra and narrow-band imaging of the 2.12 μm and 2.25 μm H_2 transitions show that the background molecular clouds exhibit both shock-excited and fluorescent H_2 emission. The shocked component exhibits small-scale, clumpy structure with large intensity variations (Bally et al. 2011) while the fluorescent component tends consist of large-scale filaments

with a relatively constant surface-brightness e.g. (Usuda et al. 1996).

Figure 1 shows the locations of the three near-IR fields observed in the NAP complex. These data reveal a large collection of protostellar jets and outflows emerging from various dense clumps in the NAP cloud complex. Figure 2 shows the 1.1 mm BGPS map with their radial velocities. The column densities of clumps associated with NGC 7000 were determined from the BGPS 1.1 mm fluxes using an assumed dust temperature of 20 K and the formulae given in Aguirre et al. (2011) and Bally et al. (2010). The areas in which column densities were estimated are shown in Figure 3. Clump radial velocities and line-widths were measured with the 10-meter Sub-Millimeter Telescope on Mt. Graham using the J = 3-2 transition of HCO^+. The abundance of shock-excited H_2 features and Herbig-Haro objects place constraints on the amount of recent star formation in each 1.1 mm clump. While some BGPS clumps are relatively inactive, others burst with outflow activity; the former objects may be in a less evolved evolutionary state than the latter. Furthermore, the locations of these outflows and associated source stars relative to the W80 ionization fronts provide clues that can differentiate between triggered and pre-existing star formation that was uncovered by the expanding HII region. Figure 4 shows the fields of view observed in the near-infrared superimposed on *Spitzer* Space Telescope images obtained at 24 μm (red), 8 μm (green), and 4.5 μm (blue) with BGPS contours superimposed and suspected massive stars marked. All coordinates discussed in this papers are given as J2000.

2.1. NEWFIRM Near-Infrared Images

The new observations reported here were obtained during 30 October to 5 November 2009 using the NEWFIRM near-IR imaging camera (Probst et al. 2008) on the 4-m Mayall telescope at Kitt Peak National Observatory. Each observation of the "Pelican" and the "Gulf-of-Mexico" fields (Figure 1) consisted of a dithered set of 11 separate exposures with offsets of up to 100″ from the nominal pointing center to fill-in the gaps in NEWFIRM's four 2048 by 2048 pixel focal plane arrays. Each reduced image has a field of view 29′ × 29′ with a scale of 0.39″ per pixel. For observations of the "Atlantic" field, larger offsets were use and resulted in a roughly 41′ × 42′ field being imaged.

Observations were obtained through 1% narrow-band filters centered on the 2.122 μm S(1) line in the ro-vibrational spectrum of H_2 and the 1.644 μm line of [Fe II] using exposure times of 180 seconds per frame to give a total exposure time per pixel of 33 minutes. Broad-band images for continuum subtraction were taken through standard broad-band J, H, and K_s filters using exposure times of 30 seconds per frame and the same dither pattern used for H_2 imaging to provide a total exposure time of 5.5 minutes per pixel. However, during these

exposures, the weather conditions were variable with occasional clouds. As a result, only cosmetically poor K_s images were obtained in the Gulf of Mexico region. Although of sufficient quality to distinguish line emission from reflection nebulae, these broad-band images did not enable continuum subtraction of the narrow-band images in this field. Continuum subtracted images were generated only in the Pelican and Atlantic regions.

The images presented here were reduced using the NEWFIRM Quick Reduce Pipeline (Daly et al. 2008). The pipeline extracts a sky image by median combination of an unregistered stack of images and then subtracts this sky frame from each image. Dome flats were used to flat-field individual images which were then registered and median combined. Stars in the 2MASS catalog were identified automatically on the images and used to remove optical distortions inherent in the re-imaging optics of NEWFIRM and to establish a World Coordinate System (WCS) for each combined frame. The mean flux of all identified 2MASS stars in the field are used for flux calibration.

The K_s images were registered to the narrow-band H_2 images with sub-pixel precision. The K_s intensity scale was adjusted by eye to match the average fluxes of stars in the corresponding narrow-band image and subtracted from it to produce a continuum subtracted narrow-band image. Variations in the point spread function between broad and narrow-band images sometimes resulted in imperfectly subtracted stars. In order to preserve the H_2 morphology, we did not alter the image PSFs to address this issue.

2.2. Bolocam 1.1 mm Continuum from Cool Dust Clumps

The observations reported here were obtained with Bolocam[1] between June 2005 and July 2007 on the Caltech Submillimeter Observatory (CSO) 10-meter diameter telescope. Bolocam (Glenn et al. 2003) is a 144-element bolometer array with between 110 to 115 detectors working during the observations reported here. The instrument consists of a monolithic wafer of silicon nitride micromesh AC-biased bolometers cooled to 260 mK. All data were obtained with a 45 GHz bandwidth filter centered at 268 GHz ($\lambda = 1.1$ mm) which excludes the bright 230 GHz J=2-1 CO line. However, as discussed in Aguirre et al. (2011), the effective central frequency is 271.1 GHz. The individual bolometers are arranged on a uniform hexagonal grid. Each bolometer has an effective Gaussian beam with a FWHM diameter of $31''$, but the maps presented here have an effective resolution of $33''$ due to beam-smearing by the scanning strategy, data sampling rate, and data reduction as discussed by Aguirre et al. (2011). Full details of the Bolocam Galactic Plane Survey (BGPS) are presented in

[1]http://www.cso.caltech.edu/bolocam

(Aguirre et al. 2011). In this paper, data from the BGPS Second Data Release (V2.0) are used Ginsburg et al. (2013). The resulting data are available to the public from IPAC/IRSA at http://irsa.ipac.caltech.edu/data/BOLOCAM_GPS.

The BGPS data can be converted into estimates of dust and gas column density and mass using the methods outlined in Bally et al. (2010).

2.3. Sub-mm Spectroscopy from the Mt. Graham 10 meter Sub-Millimeter Telescope

Observations of the J = 3-2 transitions of N_2H^+ and HCO^+ were conducted with the Heinrich Hertz Submillimeter Telescope on Mount Graham, Arizona as part of a survey of BGPS clumps (Schlingman et al. 2011; Shirley et al. 2013). The data were taken over the course of 44 nights beginning in February 2009 and ending in May 2011 with the ALMA Band-6 dual-polarization sideband-separating prototype receiver in a 4-IF setup. With this setup, both the upper and lower sidebands (USB and LSB, respectively) are observed simultaneously in horizontal polarization (H_{pol}) and vertical polarization (V_{pol}) using two different linearly polarized feeds on the receiver. The receiver was tuned to place the HCO^+ J = 3-2 (267.5576259 GHz) line in the center of the LSB. The IF was set to 6 GHz, which offsets the N_2H^++ J = 3-2 line (279.5118379 GHz) in the USB by +47.47 km s^{-1}. The signals were recorded by the 1 GHz filterbanks (1 MHz per channel, 512 MHz bandwidth in 4-IF mode; LSB velocity resolution $\Delta V_{ch} = 1.12$ km s^{-1} and USB velocity resolution $\Delta V_{ch} = 1.07$ km s^{-1}) in each polarization and sideband pair (V_{pol} LSB, V_{pol} USB, H_{pol} LSB, H_{pol} USB). 133 positions were observed in the NGC 7000 NAP complex. Figure 2 shows the 1.1 mm dust continuum image from BGPS with the radial velocities of a representative sub-sample of clumps marked. While most clumps (those marked in red in the electronic versions of the figures) have clump radial velocities between −10 and +10 km s^{-1} seen in HCO^+ in the NAP complex, others (those marked in blue in the electronic version of the figures) have LSR velocities outside of this range and are presumed to be background clumps.

3. Results

3.1. The Pelican Region: A Quadrupolar jet and Fluorescent Edges

Figures 5 and 6 show the 27′ field containing the Pelican Nebula (IC5070) ionization front and the molecular cloud that lies to its northwest. Contours of dust continuum emission at a wavelength of 1.1 mm are superimposed in Figure 6. As discussed in Aguirre et al. (2011);

Ginsburg et al. (2013), the 1.1 mm BGPS data are high-pass filtered and do not trace structure on scales larger than about 3′ to 5′. Thus, these data emphasize dense clumps and cores. The locations of the Herbig-Haro (HH) objects found by Bally & Reipurth (2003) are marked by squares in Figure 6. Suspected shock-excited sources of H_2 emission are shown with circles and numbers which correspond to the entries in Table 1. Several clusters of H_2 shocks in the Pelican region can be clearly associated with coherent outflows; these are labeled as Molecular Hydrogen emission-line Objects (MHOs) and given numbers 3400 through 3412 (C. J. Davis; private communication. See http://www.astro.ljmu.ac.uk/MHCat/ for the catalog and list of criteria used to define MHOs).

The most striking feature of Figure 6 is the presence of extended filamentary H_2 emission along the southeast-facing edges of the molecular cloud with a relatively constant intensity. We infer that these glowing cloud edges trace UV-excited fluorescent H_2 emission and indicate the direction of UV illumination. Several prominent protrusions ("elephant trunks" or "pillars") extend from the main cloud towards the southeast and provide additional indicators for the location of the exciting stars of the W80 HII region. The irradiated jet HH 555 (Bally & Reipurth 2003) is located at the eastern tip of the longest protrusion near the center left of the image. Guieu et al. (2009) found a source at 70 μm in *Spitzer* Space Telescope images at the base of the jet. The associated clump shadows the elephant trunk which points at Straižys & Laugalys (2008) star number #7 (Figure 1), one of the two massive stars with spectral type O5, located at a projected separation of about 50′ ($\sim$ 8 pc) from the Pelican ionization-front. While the overall orientation of the protrusion near HH 568 along the southeast corner of the Pelican point south of this stars's location, individual parts of this tongue, along with a number of isolated cometary clouds at the bottom of Figure 6 clearly point at star number #7. Thus, this O5 star is the most likely source of illumination of the Pelican Nebula.

Several 1.1 mm clumps and cores in the projected interior of the Pelican Nebula dust cloud northwest of the fluorescent H_2 emission associated with its ionization fronts also exhibit elongated and cometary morphologies, suggesting that they too have been impacted by illumination from the massive stars number #7 and #8, the Comerón & Pasquali star (Straižys & Laugalys 2008). These clumps may be situated behind the Pelican cloud where they are exposed to ionizing radiation. However, the lack of obvious fluorescent H_2 edges as seen near most of the Pelican Nebula ionization fronts raises the possibility that they are insulated from ionizing radiation. These 1.1 mm clumps may have been shaped by non-ionizing, softer UV or visual radiation fields that can penetrate several magnitudes into the cloud. That some of these clouds (e.g. the cloud containing MHO 3401) point towards star #8 and not star #7 implies that star #8 may be older, and has influenced the structure of W80 for a longer time. The overall elongation of the protrusion near HH 568 in the southeast

is consistent with this interpretation.

Figure 6 shows three groups of MHOs; three MHOs are located in an east-west chain near the top of Figure 6 (MHO 3400, 3401, and 3402). A second group is below the center of the image just north of HH 567. Finally, the third group is associated with the 1.1 mm cometary clumps near the bottom of Figure 6. Figures 7 and 8 shows details of the MHOs located at the top of Figure 6, MHOs 3400, 3401, and 3402. Coordinates of the various features shown in the figure are tabulated in Table 1.

MHO 3400, A Point-Symmetric Pair of Jets Emerging at Nearly Right Angles: The two most spectacular flows in the Pelican Nebula region, collectively MHO 3400, emerge from an infrared source embedded within a compact 1.1 mm core (Figure 7). An east-west jet emerges at PA $\sim 100^{\circ}$ from this star and a north-south jet comes out at PA $\sim 25^{\circ}$. Both knotty jets exhibit S-shaped, point-symmetry about the source, indicating a possible counter-clockwise precession of the jet axes. Each lobe of each jet contain approximately four bright knots within $1'$ of the source. The mean projected spacing of $15''$ corresponds to a physical separation of 1.6×10^{17} cm (0.05 pc). For a flow speed of 100 km s^{-1} typical of the inner portions of similar outflows, the time between subsequent ejections is about 500 years. Reipurth (2000) suggested that knots in HH jets may be produced by periastron passages of eccentric binaries. If 500 years is the orbital period of a pair of 1 $M_{\odot}$ stars, their typical separation would be about 10^{15} cm (70 AU), corresponding to an angular separation of $0.09''$.

A pair of distant, faint knots, W4 and E4 may mark the most distant shocks in the east-west jet in MHO 3400. N5 may trace the most distant shocks powered by the north-south jet. These knots are located at projected distances of 2 to $3'$ (0.3 to 0.5 pc) from the source. Assuming an ejection velocity of 30 km s^{-1}, a typical flow-speed for H_2 shocks and HH objects located at such distances from their sources, the dynamic ages of these shocks are about 1.0 to 1.5×10^4 years.

The MHO 3400 jet join the relatively rare class of twin jets from (presumably) multiple protostar systems in which each member powers a jet emerging at large projected angles. Other examples of mis-aligned flows include the HH 111/ HH121 system in Orion (Gredel & Reipurth 1994) and the flows in L723 (Carrasco-González et al. 2008). Outflows emerging at large angles from a multiple star system indicate that the spin-axes of circumstellar disks are misaligned. The S-shaped symmetry of the MHO 3400 jets likely indicate that the circumstellar disks surrounding each protostar experience forced precession, causing their bipolar jets to change orientation. Non-coplanar disks can result from dynamical interactions in non-hierarchical multiple star systems or from formation of the multiple star by capture (Moeckel & Bally 2007a,b). Such multiple star system N-body interactions may be common

among young stars (Reipurth et al. 2010).

Source 3 in Figure 7, IRAS 20485+4423, has fluxes of 1.9, 4.3, 46, and 316 Jy at 12, 25, 60, and 100 μm while Akari (Ishihara et al. 2010) reports a 160 μm flux of about 103 Jy. The star, visible in the near-IR and embedded in BGPS clump G084.713+00.336 is one of the half dozen most luminous YSOs in the Pelican region and is likely destined to be a moderate-mass star.

MHO 3401 in the cometary cloud IRDC G84.656+0.383: Three H_2 knots, E1, W1, and W2, emerge at position angle (PA) $\approx 130^\circ$ from a prominent 1.1 mm BGPS clump (G084.662+00.388; the millimeter wave counterpart of IRDC G84.656+0.383) which exhibits a cometary tail towards the northwest. The three knots are not co-linear; their locations suggest that the flow suffers a mild deflection towards the north or precession. The large circle (#10 in Table 1) below MHO 3400 marks the location of a possible bow shock associated with MHO 3401. High-resolution spectroscopy is needed to determine if this feature is indeed a shock or a fluorescent cloud edge.

MHO 3401 is embedded in a cometary clump and infrared dark cloud (IRDC) in the Pelican field, G84.656+0.383, seen in silhouette at 24 μm and shorter wavelengths. It contains two highly embedded protostars marked by the black circles and numbered 1 and 2 in Figure 7. YSO1, located below the axis defined by MHO 3401 E1, W1, and W2 in Figure 7, is visible in the *Spitzer* IRAC 4.5 to 8 μm bands but invisible at 24 μm. YSO2, located in the core of the IRDC between MHO 3401 E1 and W1 in Figure 7 is the more likely candidate source of this outflow. It is seen as a faint, conical reflection nebula opening towards the northwest and MHO 3401 components W1 and W2 in the *Spitzer* 4.5 μm image, a dim point source much fainter than YSO1 in the *Spitzer* 8 μm image, and the dominant point source in this IRDC at 24 μm. YSO2 is visible at 70 μm in both the *Spitzer* and Herschel Hi-GAL 70 μm images and peaks in the 160 μm band. From these colors, we infer that YSO2 is a low luminosity Class 0/I protostar while YSO1 is probably a Class I/II object which exhibits no evidence for outflow activity in the near-IR.

MHO 3402: This complex of bright, compact shocks is located near the Pelican ionization-shock front (Figure 8). MHO 3402 consists of a sub-arcminute chain of knots emerging from a tight aggregate of stars and a bright far-IR to sub-millimeter protostar embedded within a cometary 1.1 mm BGPS clump, G084.754+00.258, that points towards star #7. The IRAS catalog lists a source which is not point-like (IRAS R2049+4421) with a 100 μm flux of 127 Jy. The *Spitzer* images reveal a small cluster of about a half-dozen stars visible from 3.5 to 8 μm that correspond to the brightest 2 μm stars. However at 24 μm, the brightest source by far is embedded in the clump near the location of H_2 knot MHO 3402 W3 (black circle in Figure 8 and labeled 'IRS 4'). This is the only YSO in this region visible in the Herschel

Hi-GAL 70 μm images. It is listed in the WISE satellite all-sky data release (Cutri et al. 2012) as J205046.59+443323.1. The NEWFIRM K_s image shows a compact 8″ diameter bipolar reflection nebula surrounding this YSO with a position angle of 45°, similar to the orientation of the flow defined by a line connecting MHO 3402 W1, W2, and W3. The images suggest that this source drives a jet consisting of H_2 knots 3402 W1, W2, and W3. The chain consisting of MHO 3402 E1 through E4 may trace an additional flow from this small aggregate of YSOs. Knot MHO 3402 E1, a southwest-facing bow shock, is by far the brightest. There is no *Spitzer* source near its location. Thus, it is unclear which YSO in this aggregate is the driving source. A 2 μm star located about 5″ northeast of MHO 3402 E1 is a potential source. Knots E2 and E3 may trace another flow from the star located about 5″ southeast of knot E1. This star has been identified as a YSO by Guieu et al. (2009) based on *Spitzer* photometry.

3.1.1. MHOs in the southeast portion of the Pelican Nebula:

The extensive network of fluorescent filaments along cloud edges make the identification of shock excited emission difficult in this region. Two criteria were used to select and mark candidate MHOs. Features which stand out because they have higher surface brightness than nearby filaments, or those which have very different morphologies (e.g. bow-shapes, or isolated knots along axes defined by other candidate MHOs) are marked as MHOs. Individual clusters of knots are grouped and given MHO numbers. Admittedly, these criteria are highly subjective. These criteria result in the identification of several groups of compact knots of H_2 emission in the southeast corner of the Pelican Nebula in the cloud interior (Figure 9). Spectroscopy is required to confirm the shock nature of these objects.

MHO 3403: HH 567, the brightest HH object in the Pelican Nebula Region (Bally & Reipurth 2003), is associated with object 21 and 22 in Table 1. As shown in Figure 9, these two H_2 knots are located close to and point to a bright *Spitzer* source visible at 3.5 to 24 μm at 20:50:36.8, +44:21:39 (IRS 7a) which is likely the driver of HH 567 and the associated H_2 shocks. Several additional filaments and knots of H_2 are located southwest of object 21. However their nature (shocks or fluorescent edges) remain unclear.

MHO 3404: Knots 23, 24, 25, and 26 form a chain extending about 2′ northwest of a faint 24 μm *Spitzer* source IRS 7c (Figure 9) at J2000 = 20:50:34.8, +44:22:23. This chain is designated MHO 3404.

MHO 3405: MHO 3405 is the molecular hydrogen counterpart of the irradiated jet HH 555 (Bally & Reipurth 2003) emerging from a prominent pillar extending east of the

Pelican ionization front. The north-south ridge of H_2 emission at the eastern tip of the pillar (see Figures 6 and 9) traces the surface of the jet. The surface layers of the pillar are also aglow with slightly fainter H_2 emission. It is unclear weather the H_2 emission associated with the HH 555 jet surface is fluorescent or traces shocks. However, the H_2 surface brightness is similar to the Pelican cloud edges, suggesting that the fluorescent mechanism dominates.

MHO 3406: Spitzer source IRS 8 (Figure 9), corresponding to IRAS 20489+4410, is the brightest YSO in this portion of the Pelican cloud at 24 μm. Knot 27 located about 20″ south and elongated towards this YSO is located about 45″ east of HH 567. Knots 28 and 29 extend about one arcminute north of the IRAS source. These three knots constitute MHO 3406.

MHO 3407: Knots 30, 31, and 32 form a southeast to northwest chain whose axis passes through IRS 14, a dim IR source visible at wavelengths of 70 μm and longer in the Herschel data. Each of these three knots is elongated along the line defined by their positions. This chain constitutes MHO 3407.

MHO 3408: A pair of knots, objects 33 and 34 about 50″ and 120″ southwest of IRS 13 at 20:50:27.5, +44:23:29 forms MHO 3408. A faint knot in between but closer to object 33 may also be shock excited. Knots 24 and 32, grouped with MHO 3404 and MHO 3407 respectively, also lie along a line defined by MHO 3408, making groupings of knots into flows in this region highly uncertain.

MHO 3409: MHO 3409 consist of a pair of knots, 35 and 36 located north of IRS 6 at the top of Figure 9.

MHO 3410: A chain of irradiated HH objects, HH 563 to 565 extends south from IRAS 20489+4406 (IRS 11) in Figures 6 and 9 (Bally & Reipurth 2003). This infrared source is the brightest 70 μm YSO in the Pelican region. Objects 38, 37, and 36 are located along the axis expected for the counterflow associated with HH 563 to 565. Object 39 is located south of IRS 11 half way between HH 565 and the infrared source. This is MHO 3410. The *Spitzer* 3.5 μm images shows a reflection nebula extending north-south from this YSO, providing support for the suggested connection between this IRAS source, HH 563 to 565 (see Figure 6) and H_2 knots.

MHO 3411: A bright, compact H_2 knot located east of the axis defined by MHO 3410 and the HH 563-565 chain is MHO 3411 (object 40 in Table 1).

MHO 3412: Finally, MHO 3412 (object 41 in Table 1) is a small bow-shaped H_2 knot located on the axis of a small 2 μm reflection nebula embedded within the tip of a small cometary globule located in the southwest corner of Figures 5 and 6.

3.2. Low Level Star Formation Activity in the Atlantic

Figure 4 shows that the "Atlantic" field about a degree due east of the Pelican Nebula contains two bright infrared nebulae in the portion of the L935 dark cloud which separates the Pelican Nebula from the North America Nebula. Comparison of Figures 1 and 4 indicates that these IR-nebulae are completely obscured at visual wavelengths. The negative radial velocities of molecular gas associated with the northern object in Figure 2 (-31 to -37 km s^{-1}) indicate that it lies far behind the NAP complex. However, clumps in the vicinity of the IR-nebula near the center of the"Atlantic" field and located close to star number 4 in Figure 1 and labeled "Atlantic main" in the 1.1 mm BGPS image (Figure 3) have radial velocities indicating a possible association with the NAP. This IR-nebula contains a $6'$ diameter HII region, G085.06−00.16, with a 5 GHz flux of about 1 Jy along with a compact cluster of stars seen in the infrared images. The Planck Early Release Compact Source Catalogue (Planck Collaboration et al. 2011) includes a $5'$ diameter source with a 100 GHz flux of about 5 Jy.

The IRAS point source catalog does not list any entries near the "Atlantic main" IR-nebula G085.06-00.16,. However, a search with Visier finds two bright 60 and 100 μm sources listed in the IRAS serendipitous survey catalog (Kleinmann et al. 1986); IRAS 20518+4420 and IRAS 20519+4420 with 60 μm fluxes of about 750 Jy. The 2MASS survey lists many near-IR sources, with the brightest one identified as 2MASS 20534117+44311378. This source is marked in Figures 10 and 11.

The Bolocam source catalog Bolocat lists five 1.1 mm clumps in the "Atlantic main" region within a $5'$ radius of 20:53:40.9 +44:31:34. As shown in Figure 2, all have radial velocities between V_{LSR} = -3.3 and -5.7 km s^{-1}. The NEWFIRM near IR images (Figure 10) show that the associated cloud is cometary with fluorescent edges facing towards the southeast, indicating illumination from this direction.

The 8 and 24 μm *Spitzer* images reveal cometary features along the rim of the HII region that point toward the star cluster contained in the IR-nebula. Thus, the OB star (or stars) responsible for the ionization of the HII region and the bright mid- to far-IR emission from its immediate surroundings is suspected to be located within a few arc seconds of 20:53:42.4, +44:31:54.

Figure 10 shows a non-continuum subtracted, narrow-band H_2 image of the region. Several compact isolated H_2 knots are evident in Figure 10 and may trace shocks from outflows associated with young stars in this compact cluster (Table 2).

MHO 3413 and MHO 3415: The brightest H_2 feature, MHO 3413 in Table 2, is located near the south rim of the cometary cloud. It is unusual in that it exhibits a prominent

chain of knots in the [FeII] line at 1.644 μm (Figure 11) consisting of knots 1 though 6 in Table 2. Only knot 1 is visible in H_2, the rest are only seen in [FeII] (Figure 11). However, the relatively isolated H_2 feature, MHO 3415 (knot 11 in Table 2 and Figures 10 and 11) near the upper-left corner of Figure 10 is located within 1 degree of the axis of this [FeII] jet. MHO 3415 may therefore trace an outlying shock in this flow, in which case it is a candidate parsec-scale outflow. The source may be a *Spitzer*-detected 3.6 to 8 and 24 μm YSO at 20:53:30.9, +44:30:03 located midway between [FeII] knots 1 and 2. Although this YSO is visible in the H and K_s images, its flux increases with increasing wavelength up to at least 24 μm. The [FeII] image shows a jet extending from this source to knot 1.

MHO 3414: This MHO contains four knots (7,8,9 and 10 in Table 2 and in Figures 10 and 11) which form a chain which may trace a single outflow. A 24 μm-bright *Spitzer* YSO located at 20:53:36.5, +44:34:33 is located a few arcseconds southeast of knot 8 and may be the driving source of this southeast-northwest oriented flow. A faint 2.2 μm reflection nebula connects this knot to the *Spitzer* YSO, supporting the interpretation that this source drives this outflow.

MHO 3416: Finally, a faint pair of H_2 and [FeII] dominated knots are located about 1.5′ west of the star 4 (Straižys & Laugalys 2008) which they list as a candidate massive star with spectral type O9 to B0. The axis defined by the two knots also points back towards the 24 μm *Spitzer* YSO marked by the 'X' North of [Fe II] knot 2 in Figure 10 potentially associated with MHO 3414. Thus, the source is unclear.

3.3. The Gulf of Mexico Region

The Gulf region shown in Figures 12 through 22 is the most active site of on-going star formation in the NAP region. This region contains many MHOs, HH objects, IRAC-identified Class I, II , and III YSOs, and highly embedded Class 0 or I YSOs seen mostly at 24 and 70 μm that could be drivers for the various shocks. Early surveys for Hα emission line and flare stars (Herbig 1958; Welin 1973) identified over 60 young stars. The recent study by Armond et al. (2011) identified 35 HH objects (HH 636 through 663 and HH 952 through 958), 5 possible HH objects, and 30 new Hα emission line stars. The *Spitzer* IRAC and MIPS images, combined with 2MASS photometry (Guieu et al. 2009; Rebull et al. 2011) led to the identification of about 2,076 YSOs in the NAP complex of which 375 are located in the 'Gulf of Mexico'. Table 3 lists over a hundred individual shocks many of which have complex substructure.

Figure 12 shows the full field of view H_2 image of the Gulf region which can be subdivided

into three sub-regions: The region 'Gulf SW2' (Figure 13) consists of the collection of bright BGPS clumps on the right-side of Figure 12. In Figure 3, these clumps are further divided into 'SW2 main', 'SW2 SE', and 'SW2 S' for determination of column densities and masses. The region dubbed 'Gulf SW1' (Figure 15) is associated with the compact BGPS clump and an IRDC visible in silhouette at wavelengths of 24 μm and shorter (G84.963-1.173) located just above the center of Figure 12. The northeast portion of the Gulf located in the upper-left portion of Figure 12 is dubbed 'Gulf core' (Figures 16 through 19). Grouping HH objects and H_2 shocks into coherent outflows is difficult owing to the large number of individual features and the high density of YSOs. Below, the discussion of MHOs proceeds roughly from southwest to northeast.

3.3.1. A Giant Outflow from the Most Massive Clump in the Gulf: 'SW2 main'

The brightest and largest 1.1 mm BGPS clump in the NAP complex ('SW 2 main'; Figure 3) is located about 15′ southwest of the very active region of star formation in the 'Gulf core' (consisting of 'core E' and 'core W' in Figure 3). Although this large and structured 1.1 mm clump exhibits three to five times more total 1.1 mm emission, and is therefore likely to be more massive by the same factor than the highly active complex at the northeast end of the Gulf, it exhibits a much lower level of outflow activity. The 'Gulf SW2' region contains several reflection nebulae, several dozen *Spitzer* / IRAC YSOs, 24, and 70 μm sources, and about a dozen H_2 shocks and contains the largest outflow detected in the NAP complex, MHO 3417 (Table 3).

The two brightest H_2 features in the 'SW2 main' clump consist of oppositely facing bow shocks located in the upper-right and lower-left in Figure 13. The northern bow (H_2 feature 1 in Table 3) was detected by Armond et al. (2011) at visual wavelengths and designated HH 953. The southern bow (H_2 feature 5), HH 954, is much fainter at visual wavelengths than the northern shock. These two shocks are symmetrically placed about the 1.1 mm peak of 'Gulf SW2'. Several faint H_2 knots (objects 2,3,4, 6, and 7) lie on or near the axis defined by this flow. This giant flow is designated MHO 3417 in Table 3. The projected separation between HH 953 and 954 is about 10′ in projection, or about 1.6 parsecs at the distance to the NAP complex.

The two brightest 24 and 70 μm sources in 'Gulf SW2' in the *Spitzer* data are located on the flow axis. The northern source, IRS 1 (Table 3), is brighter at 70 μm and more obscured. H_2 knot 2 (Table 3) is located about 30″ northwest of the location of IRS 1. The southern source, IRS 2 (Table 3), is the brightest source at 8 μm in the *Spitzer* images. A 2 μm source and faint reflection nebula (R1 in Table 3) on the north side of this clump is

evident in the NEWFIRM data. It is unclear which IR source is the driver of the MHO 3417 HH 953/954 outflow. Zhang et al. (2011) suggests that a massive star is forming in the 'SW2 main' clump. But, it is not clear which of the mid-IR sources may be the suspected massive star.

3.3.2. Other MHOs in Gulf 'SW2 main'

MHO 3418 (Figure 13) consists of faint H_2 knots (8 and 9 in Table 3) located near and southeast of a 24 and 70 μm source embedded in the southern BGPS peak in 'SW2 main'. This far-IR source is designated IRS 3 in Table 3. A faint H_2 jet extends from this source to reflection nebula R3. It is possible that knot 8 traces a small outflow from a deeply embedded source in R3 while knot 9 is powered by IRS 3. There is a faint H_2 knot about 15″ east-northeast of the 70 μm source. Thus, MHO 3418 may consist of several small flows from highly embedded low luminosity YSOs.

MHO 3419 (Figure 13) consists of a bright H_2 arc (number 10 in Table 3) located about 50″ due north of reflection nebula R2 and the IR source IRS 4 and about and 30″ southwest of IRS 5. IRS 5 is much brighter at 24 μm (it is the second brightest source in 'SW2 main' at 8 μm) than IRS 4. The source of this shock is unclear.

Figure 14 shows the BGPS clumps SW2 SE and SW2 S and MHOs 3420 through 3424. MHO 3420 is a compact, east-facing bow shock (number 11 in Table 3) located in between the two dust filaments SW2 main and SW2 SE (Figure 3) in the Gulf SW2 clump.

MHO 3421 is a bright bow-tie shaped compact H_2 feature (knot 12) and a filament (knots 13 and 14) associated with a compact aggregate of a half dozen YSOs embedded in the north-end of BGPS clump 'SW2S' (Figure 3). The H_2 features are visible in the *Spitzer* IRAC 4.5 μm images and thus are 'extended green objects' (EGOs). Faint [SII] emission is also seen from knot 12 in the images presented by Armond et al. (2011) and it is here designated as HH 1087.

MHO 3422 (Figure 14) consists of H_2 knots 15 and 16 located southeast of reflection nebulae R5 and R6 in the 'SW2 SE' clump. A bright 70 μm source, IRS 7, is located at the southern tip of this clump about 30″ north of the K-band reflection nebula R5. R6 is associated with a 24 μm source.

MHO 3423 consists of a pair of faint H_2 knots (17 and 18 in Table 3) located south of the north-end of BGPS filament 'SW2 SE' which contains several embedded IR sources.

MHO 3424 (Figure 14) consists of a chain of faint H_2 knots (19, 20, 21 in Table 3)

aligned along a east-southeast to west-northwest axis located in the space between BGPS filament 'SW2 SE' and 'SW2 main' and north of MHO 3423. It is possible that the knots in MHO 3423 and 3424 trace flows from the IR sources in the 'SW2 SE' filament.

MHO 3425 (Figure 13) consists of a diffuse H_2 feature located about 3′ east of the 'SW2 main' clump. Its morphology may indicate a south-facing shock.

Given the relatively large number of *Spitzer* detected YSOs, and the presence of at least one large outflow, the relative paucity of H_2 features in Gulf 'SW2 main' compared to the Gulf 'core E' and 'core W' regions may be due to its relatively large column density and foreground obscuration which may hide some shocks. As discussed above, the 3.6 Jy peak emission in a 33″ beam at $\lambda = 1.1$ mm implies an H_2 column density of $N(H_2) = 7.2 \times 10^{22}$ cm^{-2} assuming a dust temperature of 20 K, corresponding to a visual extinction, $A_V \approx 36$ magnitudes, or larger if the dust temperature is lower.

3.3.3. Outflows from the Gulf 'SW1' Region

Gulf 'SW1' is an opaque IRDC, G84.963-1.117, located about 250″ south of the bright infrared reflection nebula R10 (Figure 16) embedded in the Gulf of Mexico 'Gulf core' region. It is seen in silhouette at 24 μm and shorter wavelengths.

A 70″ long string of 5 knots (23 through 27) emerge from a small cloud seen as an IRDC at the northwestern end of the Gulf SW1 region; this is MHO 3426. An infrared source visible at 8, 24, and 70 μm (IRS8 in Table 3) is located at the position of knot 24. Though not listed in the YSO compilation of Guieu et al. (2009), its location at the base of a compact 10″ long H_2 jet makes it likely to be another highly embedded Class 0 YSO. The jet is pointed at knots 25, 26, and 27 that together form a bow-shock facing east. A faint shock, knot 23 is seen on the west side of the source. This morphology suggests that the east side is the blue-shifted, approaching side of this outflow.

MHO 3427 is a 330″ long chain containing a dozen H_2 shocks (listed as 28 through 40 in Table 3) that emerge from the most opaque portion and peak of the 1.1 mm emission located near the east-end of the Gulf SW1 clump. Guieu et al. (2009) list nearly two dozen YSOs in the vicinity of this dark cloud, but none near the 1.1 mm peak. The brightest H_2 features (knots 36 and 37) appear to form an east-facing bow shock; knots 30 and 31 trace a west-facing shock.

Inspection of the *Spitzer* 70 μm image shows a dim but compact source at the location noted as IRS 10 in Figure 15 and Table 3. Although this source is not seen at 24

μm, the symmetric placement of the two oppositely oriented bow shocks suggests that the 70 μm source is a highly embedded Class 0 protostar. Future far-infrared or sensitive radio continuum searches are needed to confirm or deny the reality of this source.

A prominent 2 μm reflection nebula (R9 in Table 3) is associated with the brightest 4.5 to 24 μm source in this region. Also detected at 70 μm, this object is listed as IRS 9 in Table 3. At 2 μm, the nebula appears bipolar with a bisecting dust lane separating the brighter southern lobe from the dimmer northern lobe. The morphology may indicate the presence of a disk shadow produced by a disk with an axis at position angle of 210°. There are no H_2 shocks or HH objects along the suspected axis of this disk.

3.3.4. A Burst of Outflows from the 'Gulf core' Region

The 'Gulf core' region consisting of BGPS clumps 'core E' and 'core W' in Figure 3 contains the highest concentration of outflows in the NAP complex. The high density of HH objects and H_2 shocks makes the identification of individual outflows difficult as there may be multiple overlapping outflows along many lines-of-sight. Figures 16 through 19 show our H_2 image and optical wavelength Hα and [SII] images of the 'Gulf core' region from Armond et al. (2011). Comparison with the Hα and [SII] images indicates that the several dozen H_2 features shown in Figure 16 are generally not the same as the shocks traced at visual wavelengths. Most of the H_2 features trace portions of outflows that are not visible in Hα and [SII], and therefore provide complementary data. While the HH objects mark shocks in regions suffering relatively low-extinction (A_V less than a few magnitudes), the MHOs can be seen through an order of magnitude larger extinction. Thus, it is likely that the visual-wavelength emission lines mostly trace the approaching, or blue-shifted portions of outflows, while the MHOs trace both the approaching lobes and their counter-flows. The absence of MHOs at the locations of some HH objects may indicate either the complete dissociation of H_2 by shocks propagating through the cloud, or an absence of H_2 which indicates that the shocks are impacting atomic gas outside the molecular cloud.

Clusters of shocks in close proximity that may trace outflows are given MHO numbers. However, future observations may show that some of these groupings represent overlapping flows that are unrelated. The grouping into outflows is especially ambiguous in the 'Gulf core' region due to crowding and confusion.

MHO 3428, (near the northeast edge of Figure 15) located about 2.5′ northeast of Gulf 'SW1', consists of a pair of faint H_2 knots that are molecular counterparts to HH 639. Knot 41 in Table 3 is associated with the brightest part of this HH object which appears to trace

a flow propagating at PA $\sim$ 130 to 40°. MHO 3429 is an isolated knot associated with HH 638 and may be part of the same flow as MHO 3428/HH 639.

MHO 3430 consists of two H_2 knots (knot 44 and 45 in Table 3) which are the near-IR counterparts of HH 636 located along the eastern rim of the large near-IR reflection nebula R10. The southern H_2 knot (44) is a 30″ diameter H_2 feature resembling a south-moving bow shock. The northern knot (45) is located along the eastern rim of HH 636 and coincides with a bright [SII] feature. One of the brightest 8, 24, and 70 μm sources, IRS 11, located at the northern end of HH 636 / MHO 3430, is associated with the bright 2 μm reflection nebula R13.

MHO 3431, located directly north of R13 and IRS 11 contains knots 46 to 48 and may be a counterflow and near-IR counterpart to HH 637.

MHO 3432, located 30″ due west of IRS 11 is a faint collection of H_2 knots; it may be a visually obscured counterflow to HH 640 / MHO 3434.

MHO 3433 is comprised of three H_2 knots (51, 52, and 53) located 170″ to 270″ northwest of IRS 11. Knot 52 is associated with an HH object not listed in Armond et al. (2011); it is designated HH 1088.

MHO 3434 is an east-west collection of knots associated with the western part of HH 640. Knot 50 is located 6″ west of IRS 12, a mid-IR source that is redder but fainter than IRS 11 and associated with 2 μm reflection nebula R14. A fainter H_2 knot is located about 7″ east of R14/IRS 12 which is likely to be the driving source.

MHO 3435 consists of a jet-like chain of H_2 knots 54 through 60 associated with the eastern part of HH 640. It is unclear if this MHO is a part of the same flow as MHO 3434 or a separate flow, possibly powered by IRS 11. The nearly continuous H_2 emission bends south towards knots 61 and 62, east-facing bow shock 63 (associated with HH 643), and filament 65. It is also unclear if knots 61 through 65 are part of the same flow or trace shocks in other flows in the region. A very dim H_2 feature that resembles a bow shock (74 in Table 3) may also be part of this chain since there is a faint trail of H_2 emission extending back to just south of knots 64 and 65.

MHO 3436 consists of knots 66 through 71 which form a 70″ long linear chain at PA $\sim$ 34°. Knot 70 is the near-IR counterpart of HH 642. A near-IR star at 20:57:52.91, +43:53:28.4 associated with reflection nebula R17 is located near the middle of this chain. The southwestern knots 66 and 67 are much brighter than the northeastern knots, suggesting that the southwestern side of the flow is approaching.

MHO 3437 is a compact knot (72) located 17″ north of R15 associated with mid-IR

source IRS 13. The H_2 knot is the western, compact component of HH 641.

MHO 3438 is a bright H_2 shock about 5″ southwest of a star and also 25″ southwest of IRS 14.

MHO 3439 is a 2.8′ long chain consisting of knots 75 to 78. Knots 75 and 76 are bright while 77 and 78 consist of faint filaments and knots aligned with the overall southeast-northwest orientation of the flow at PA $\sim 130°$. Knot 75 is associated with a dim [SII] counterpart which appears to be an HH object (HH 1089).

MHO 3440 consists of three knots, 80 to 82 in Table 3 which are also seen in [SII] as HH 648. A faint HH object candidate is located along the axis defined by HH 648 at 20:58:01.84, +43:52:17.4 in the Subaru [SII] image indicating that MHO 3440 is a collimated flow.

MHO 3441 consists of three knots (83, 84, and 84e) that are near-IR counterparts to HH 649. The knots are connected by a faint Hα and [SII] bridge in the Subaru images.

MHO 3442 is an H_2 filament about 10″ north of MHO 3440 knot 82 and labeled as knot 82n in Table 3 and as MHO 3442 in Figure 16.

MHO 3443 is a collection of H_2 features around IRS 15. The southeastern feature (85 in Table 3) looks like a bow shock facing away from IRS 15. The western rim of the 40″ diameter H_2 feature 88 coincides with HH 647. Like MHO 3438, MHO 3443 is also in close proximity to IRS 14.

MHO 3444 consists of two H_2 knots about 1.7′ northwest of the Herbig cluster, a dense aggregate of YSOs and Hα emission line stars discovered by George Herbig Herbig (1958) embedded in the large reflection nebula complex R19 at the eastern end of the Gulf core region.

MHO 3445 consists of an H_2 filament and knot (91 and 92) about 0.7′ northwest of the Herbig cluster.

MHO 3446 is a prominent outflow extending southeast of the Herbig cluster. The FU Ori candidate HBC722 (V2493 Cyg, LkHα 188-G4) that experienced a 4 to 5 magnitude visual-wavelength flare in 2010 (Semkov et al. 2010; Miller et al. 2011; Semkov et al. 2012) is located in the Herbig cluster near the likely point of origin of MHO 3446. This region was observed with the SMA in the 1.3 mm-wavelength transitions of CO and the adjacent continuum by Dunham et al. (2012) who found a cluster of continuum sources, MMS1 through MMS7. Only MMS2 and MMS3 are associated with stars in our H_2 image; the rest have no near-IR counterparts. This indicates that the Herbig cluster contains some highly embedded sources not yet visible in the near-IR (Armond et al. 2011).

A bipolar CO outflow was detected by Dunham et al. (2012) at position angle PA $\sim$ 135° centered on the mm-source MMS3, located about 2″ from 2MASS20581617+4353310 (m_K = 13.1, m[3.6] = 11.75, m[8.0] = 8.8, m[24.0] = 3.78 mag.). The blueshifted lobe of this flow is closely aligned with objects 97 through 100; the redshifted lobe appears to be associated with object 96. However, no obvious H_2 features appear to be associated with the FU Ori candidate, HBC722.

Knots 99 and 100 in MHO 3446 are closely associated with bright knots in HH 657. However, the northern part of this HH object lies east of and has a different orientation than the flow orientation defined by knots 97 and 98. Knot 101 does not belong to either the chain of HH objects or MHOs. Knot 96, located northwest of the Herbig cluster may be a counterflow to the MHO flow axis defined by knots 97 and 98. It is likely that the various components of MHO 3446 and HH 657 trace parts of multiple overlapping flows emerging from the Herbig cluster.

MHO 3447 is a northeast facing bow and knot located about 1′ north of the Herbig cluster along the axis defined by the filaments MHO 3445.

MHO 3448 is a compact knot associated with HH 658 east of the Herbig cluster. MHO 3449 is a pair of diffuse H_2 knots southeast of HH 662.

MHO 3450 and 3451 are chains of H_2 knots at the northeast periphery of the Gulf region. MHO 3450 is centered on mid-IR source IRS 16 located a few arc seconds east of knot 109 at the location of reflection nebula R21. This is almost certainly the driving source. MHO 3451 is a north-south flow associated with HH 958 whose driving source is not obvious.

4. Clump properties

Table 4 lists the properties of the major clumps and largest cores in the NAP complex as determined from the 1.1 mm BGPS Version 2.0 maps. Figure 3 shows the regions inside which the fluxes were summed and divided by the number of pixels per CSO Bolocam beam area. In the standard Bolocam pipeline processed images, the pixels are 7″.2 in diameter and there are 23.8 pixels in each gaussian beam with a full-width-half-maximum diameter of 33″ (equivalent to a 40″ diameter top-hat beam). Table 4 lists the coordinates of the centers of each of the ovals shown in Figure 3, the total flux in each oval in Janskys, the mass enclosed in the ovals, and the major and minor diameters of the regions in arcseconds. The mass estimates assumed a uniform dust temperature of 20 Kelvin, a gas-to-dust ratio of 100, and that all clumps in the NAP complex are located at a common distance of 550 pc. A detailed description of the column density and mass-estimation method used for Bolocam

BGPS data is given in Bally et al. (2010).

In the Gulf core region, the BGPS-based mass estimates can be compared to the published 1.3 cm ammonia-based estimates (Toujima et al. 2011; Zhang et al. 2011) . The 'Gulf core' region corresponds to Toujima et al. (2011) 'sub-clumps' A1, A2 and A3 while our 'Gulf SW2' corresponds to Toujima et al. (2011) clump B. Below, their mass estimates are scaled to a distance of 550 pc (they used a distance of 600 pc).

Toujima et al. (2011) core A1 (ammonia mass of 10 $M_\odot$) corresponds to our 'core E' with a Bolocam-based mass of 32 $M_\odot$. Their A2 + A3 (ammonia mass of 24 $M_\odot$) corresponds to our 'core W' for which we estimate a mass of 64 $M_\odot$. The total mass of the 'Gulf core' region (their region A) has an ammonia-based LTE mass of 80 $M_\odot$ and a virial mass of 105 $M_\odot$ that can be compared to a Bolocam-based mass of 96 $M_\odot$. Thus, although Toujima et al. (2011) find smaller masses for their 'sub-clumps', perhaps because they associate a smaller region with each core, the overall mass estimates for our 'Gulf core' region are in excellent agreement with our Bolocam-based estimate.

The 'SW1' core is seen as a minor lump in the Toujima et al. (2011) map and no mass estimate was provided in their paper. Toujima et al. (2011) region B and our region 'SW2 main' + 'SW2 SE') have ammonia based masses of 294 $M_\odot$ to 380 $M_\odot$. For the corresponding region, the Bolocam-based mass is 596 $M_\odot$. As discussed by Zhang et al. (2011), Gulf SW2 is also known as MSX dark cloud G084.81-01.09. This object may potentially form a massive star. Zhang et al. (2011) also mapped ammonia and compared the results to Bolocam BGPS V1.0 images. Zhang et al. (2011) P1 corresponds to our 'SW2 main' clump with an ammonia mass of about 200 $M_\odot$ and BGPS mass of 477 $M_\odot$. Zhang et al. (2011) P2 with a mass 120 to 255 $M_\odot$ corresponds to our 'SW2 SE' with 119 $M_\odot$. Zhang et al. (2011) P3, P4, and P5 with a mass of $\approx$ 300 $M_\odot$ corresponds to our 'Gulf SW2 S' with a BGPS mass of only 26 $M_\odot$. Summing all of the Zhang et al. (2011) regions gives a molecular mass estimate of about 830 $M_\odot$, somewhat larger than our total mass estimate based on BGPS for the entire Gulf region. Uncertainties, intrinsic variation of the dust temperature, and different regions of spatial integration may account for these variations in the mass estimates, especially on small scales.

As shown in Figure 13, the largest outflow with the biggest H_2-bright shocks, the 9′ (1.4 pc) long MHO 3417, emerges from the relatively massive 'Gulf SW2 main' clump. As suggested by Zhang et al. (2011), the large mass of the clump and the presence of a parsec-scale outflow are consistent with the proposal that this clump is in the early stages of massive star formation.

4.1. Fluorescent Edges and Cometary Clouds Point to the Comerón & Pasquali Star

Several very long cometary clouds are located southeast of the Gulf in Figure 12 and rendered visible by their fluorescent limb-brightened cloud edges. These clouds are listed in Table 3 with the designation 'C' followed by a number (1 through 18) and marked by cyan circles in the electronic version of this paper. The longest one (C4, C5, and C6) has a length to width ratio of about 20 to 1, and can be used to locate the direction to the primary source of UV irradiation in this part of the NAP complex (Figure 20). Several other cometary clouds near the bottom center of Figure 12 (C1 through C3 and C12 through C17) also trace the direction of illumination (Figures 21 and 22). The intersection of lines extended along the orientation of these cometary clouds indicate the location of the illuminating star. These lines intersect near the location of the Comerón & Pasquali star (# 8), the O5V star located behind the Gulf (Figure 4). Thus, the orientations of cometary clouds with fluorescent edges confirm that this object is the dominant source of UV radiation in the southeastern portion of the NAP complex.

5. Discussion

5.1. The Evolutionary States of Clumps

Outflow activity, counts of IR-excess sources, and Hα emission line stars can be used to constrain the relative evolutionary states of nearby 1.1 mm BGPS clumps where the visual extinction is less than about 10 magnitudes. Stellar Hα emission from active chromospheres and accretion flows, infrared excess emission in the 1.2 to 2.4 μm and 3.6 to 8.0 μm *Spitzer*/IRAC images, the presence of HH objects and shock-excited MHOs, and sources visible only at wavelengths of 24 μm or longer trace progressively younger phases in the evolution of young stars. Highly embedded Class 0 or Class I YSOs, which tend to be younger than about 10^5 years, are most likely to power outflows and jets which excite H_2 shocks. Herbig-Haro objects tend to be powered by somewhat less embedded, older stars. As accretion onto forming stars abates, so does the power of outflow activity. Only a few stars older than about 10^6 years have associated outflows, and these tend to have low mass loss rates ($\dot{M} < 10^{-8}$ $M_\odot$) which are hard to detect except when externally ionized. However, IR-excess and stellar Hα emission can persist for many millions of years. The majority of *Spitzer*-detected IR-excess YSOs have spectral energy distributions (SEDs) indicating that they are in the Class II phase. Most of these stars are likely to be older than 10^6 years. Low-obscuration Hα emission-line stars tend to be older still. Thus, the BGPS-based mass

and the relative numbers of MHOs, HH objects, IR-excess sources, and Hα emission-line stars are indicators of dust clump evolution.

BGPS clumps with large mm-wave fluxes and few indicators of outflow activity, few IR-excess sources, and few Hα emission-line stars in their vicinity may be relatively young. On the other hand, clumps with large numbers of HH objects, Hα emission line stars, and MHOs are likely to be relatively evolved. Using this metric, the 'Gulf core' region with the highest concentration of HH objects and MHOs appears to be the most evolved region of those studied here. The number of H_2 shocks divided by the clump mass provides a quantitative estimator of outflow activity, I_{out}. The total number of catalogued H_2 features in Table 3 in the 'Gulf core' region is 73 and the BGPS mass in this region is about 96 $M_\odot$. Thus, the activity index $I_{out} = N_{MHO}/M_{dense_gas} \approx 0.76$ for the 'Gulf core' region. For the most massive clump, 'Gulf SW2 main', $I_{out} \approx 0.05$. For the 'Atlantic main' clump, $I_{out} \approx 0.06$ if the two non star-forming clumps in Table 4 are excluded. If these are included, $I_{out} \approx 0.05$. The index for the Pelican region is $I_{out} \approx 0.17$, indicating a relatively advanced evolutionary stage, though not as evolved as 'Gulf core'. For all clumps in the NAP complex excluding 'Gulf core', but including 'SW2 main' $I_{out} \approx 0.09$. If 'SW2 main' is also excluded, the remaining clumps have activity index $I_{out} \approx 0.13$.

The counting of H_2 shocks is highly subjective. Large and complex objects are counted once and given the same weight as compact isolated knots are. An area-weighted activity index may be a more robust estimator of the momentum injection rate and thus more representative of the evolutionary stage. However, a simple attempt to include the shock area of several regions in the NAP shows that the basic results will be similar. Counts of *Spitzer*-identified YSOs could also be used as a star-formation rate activity and evolutionary stage indicator. Since outflows detectable as MHOs tend to have about an order of magnitude shorter lifetimes than *Spitzer*-detected YSOs ($< 10^5$ years for MHOs; $> 10^6$ years for YSOs), outflows are expected to be a more selective evolutionary indicator.

On the basis of activity index, the most massive clump, 'Gulf SW2' appears to be the least evolved, despite containing the largest outflow. 'Gulf core' appears to be the most evolved (but still actively star-forming) region. 'Atlantic main' which also has a very low index poses an interesting situation. The presence of an IR bubble and HII region suggests that star formation has stopped in the center of this clump while the large mass of the dust in the surrounding region combined with a small number of outflow and YSOs may indicate a very early phase of star formation in the HII region surroundings.

The most massive BGPS clump in the NAP, Gulf SW2, contains the parsec-scale outflow MHO 3417 and relatively few H_2 shocks. Although there are a comparable number (many dozens) of 8 and 24 μm sources in both the Gulf core and Gulf SW2 regions, the BGPS flux

and derived mass of SW2 is about five times greater than the Gulf core. Thus, the number of mid-IR YSOs and outflows divided by the 1.1 mm flux and dust mass is at least a factor of four lower in Gulf SW2 than in Gulf core. This also suggests that Gulf SW2 is in an earlier evolutionary stage than the Gulf core region.

The large area-covering-factor of HH and MHO shocks in the Gulf core region indicates that much of the volume of this cloud is being re-processed by supersonic shocks. In the northeastern portion of the Gulf, the several dozen outflows traced by HH objects and MHOs cover about 5 to 10% of the projected area of the cloud (Figure 16 to 19). In the absence of FUV and ionization feedback from massive stars, re-processing by outflows may dominate the self-regulation of star formation and may even disrupt the clump. Such intense outflow activity has been observed in other regions such as NGC 1333 in the Perseus molecular cloud (Bally et al. 1996). Feedback from outflows has been suggested to be the dominant source of energy and momentum injection in the absence of massive stars (Li & Nakamura 2006; Nakamura & Li 2011).

As star formation abates, outflow activity weakens, and the MHOs and HH objects disappear. However the aging YSOs can still be traced by IR-excess or stellar Hα emission. The G085.06-00.16 HII region, along with most of the stars in the Rebull et al. (2011) 'Atlantic cluster' West of the HII region and East of the Pelican Nebula ionization front may be approaching post-star-forming dormancy.

5.2. Triggering?

The distribution of star formation in the clouds surrounding the NAP complex can be used to constrain the modes of star formation. Three possible modes of star formation have been proposed (Elmegreen 1998).

[1] *pre-existing, spontaneous star formation*: Star formation can occur spontaneously throughout the cloud without triggering. In that scenario, YSOs currently located at cloud edges and at the tips of elephant trunks and pillars would have formed regardless of the expanding HII region that has sculpted the local cloud morphology. The velocities of stars and associated cloud cores are expected to be uncorrelated with either the HII region velocity or with the velocity of any swept-up shell. Spontaneous star formation should also produce YSOs deep inside clouds far from impinging ionization fronts. The YSOs in the interior of the Pelican cloud, such as the sources of MHO 3400 and MHO 3401 may be examples.

[2] *Pressure-triggered gravitational collapse*: As an advancing ionization front wraps around pre-existing clumps, its pressure triggers gravitational collapse and star formation.

Stellar velocities are expected to weakly correlate with the HII region's expanding shell. As ionization exposes a clump, photo-ablation of its surface and the resulting Oort-Spitzer rocket effect can accelerate remaining gas and the embedded YSO away from the ionizing sources. Young stars will be located between the center of HII region expansion and cometary wakes or pillars. The YSOs at the heads of pillars such as the one which drives HH 555 in the Pelican Nebula may be examples of this mode.

[3] *Collect and collapse:* In 'classic' triggered star formation, clumps form from gas swept up by the expanding HII region. When enough mass is collected, the local gravitational escape speed becomes larger than the spreading velocity due to the shell expansion and gravitational collapse occurs. Forming stars will inherit the expansion velocity of the shell when it becomes unstable to its own self-gravity. For decelerating shells, YSOs will tend to outrun the shell. Precision radial velocities and proper motions of stars and gas are needed to reliably discriminate between these scenarios.

There are indications that the 'Gulf core' region is in the foreground relative to the rest of the NAP. The Pelican ionization fronts point toward the center of the HII region and various cometary clouds point toward the Comeran and Pasquali star #7, and this star is behind the 'Gulf of Mexico' region. The redshifted radial velocity of about V_{LSR} = 4 to 6 km s^{-1} indicates that the Gulf core region, which supports such a high density of YSOs and outflow activity, is plunging inward towards the NAP HII region. This is inconsistent with the collect and collapse scenario.

The Atlantic ridge portion of the L935 cloud separating the North America and Pelican nebulae is blueshifted by about 3 to 8 km s^{-1} with respect to the molecular gas in the Pelican and Gulf regions of the NAP (Bally & Scoville 1980) . This region also obscures the central part of the NAP HII region and must therefore be located in the foreground. Bally & Scoville (1980) concluded that this portion of the L935 cloud has been accelerated by the expansion of the HII region. The V_{LSR} = -4 to -6 km s^{-1} blueshift of the gas associated with the G85.06−0.16 HII region, cluster, and outflows in the Atlantic region of L935 may be consistent with the 'collect and collapse' scenario of triggered star formation. The radial velocities of the clumps in the Gulf SW1 and SW2 regions observed by Toujima et al. (2011) and Zhang et al. (2011) and by the Mt. Graham telescope N_2H^+ and HCO^+ measurements presented here ($V_{LSR} = -2.9$ to $+1.8$ km s^{-1}) are consistent with this picture since these regions are located near the projected edge of the giant NAP HII region (W80; NGC 7000) where the motions induced by HII region expansion are expected to be mostly along the plane of the sky.

The 'Gulf core' region, which supports the highest density of YSOs and outflow activity in the NAP complex, has a redshifted radial velocity of about V_{LSR} = 4 to 6 km s^{-1}(one

faint knot has $V_{LSR} = 10$ km s^{-1} in Figure 2), indicating that it may be plunging in towards the NAP HII region. There are indications that the Gulf core region is in the foreground relative to the rest of the NAP complex of clouds. The Pelican ionization fronts point toward the center of the HII region, cometary clouds point toward the Comeron and Pasquali star, and this star is behind the 'Gulf -of-Mexico' as it is highly obscured. The redshifted radial velocity of about $V_{LSR} = 4$ to 6 km s^{-1} suggests that the Gulf core region, which supports such a high density of YSOs and outflow activity, is plunging in towards the NAP HII region. This is inconsistent with the collect and collapse scenario. It is possible that the back side of the 'Gulf core' region is in contact with the high-pressure HII region, was compressed as a result, and has therefore recently experienced a burst of star formation. It may be an example of star formation in a pre-existing cloud triggered by external pressure. On the other hand, the star formation sites located a parsec or more away from the NAP ionization fronts within the Pelican Nebula cloud may be 'spontaneous' star forming events mostly unaffected by the W80 HII region.

5.3. Star Formation Efficiency in the NAP

The star formation efficiency (SFE) in the NAP can be crudely estimated by taking the ratio of the number of YSOs in each region times the median YSO mass, and dividing by the masses of the parent clumps or the total mass of molecular gas in the NAP.

The NAP complex is surrounded by a giant molecular cloud complex. Bally & Scoville (1980) found a mass of 3.0×10^4 M$_\odot$ for the clouds surrounding and lying in front of the NAP. Feldt & Wendker (1993) obtained ^{12}CO and ^{13}CO maps of the NAP finding masses (scaled from their 500 pc to our 550 pc distance) of 2.8×10^4 M$_\odot$ and 4.3×10^3 M$_\odot$, respectively. They argue that the total cloud mass is the sum of the ^{12}CO and ^{13}CO masses since the ^{13}CO line is only seen where ^{12}CO is very smooth and likely to be very optically thick. Dobashi et al. (1994) mapped ^{13}CO in the Cygnus-X region, finding a ^{13}CO mass of about 6×10^3 M$_\odot$ in the L935 region studied here. Thus, the total H_2 mass is likely to be about 4×10^4 M$_\odot$ with at least a factor of two uncertainty. The total mass of H_2 detected by BGPS is about 1.1×10^3 M$_\odot$. This is likely to be a lower bound due to the spatial filtering of the BGPS data which loses sensitivity to structure larger than approximately $5'$.

Guieu et al. (2009) used 3.6 to 8 μm *Spitzer*/IRAC to identify more than 1,600 candidate YSOs in the NAP. Rebull et al. (2011) used 24 μm *Spitzer*/MIPS to find additional objects increasing the number of candidates to over 2,000. *Spitzer* is most sensitive to young embedded Class I sources, somewhat older 'flat-spectrum' YSOs, and more evolved Class II objects with warm circumstellar disks. Assuming a median mass of 0.5 M$_\odot$, and a total

mass for the NAP of 4×10^4 $M_\odot$ implies a lower bound on the SFE of about 2% since the majority of the more evolved and presumably older Class III YSOs are likely to have been missed.

Restricting attention to the three regions of the NAP containing the largest concentration of Class I sources and all of the BGPS clumps gives somewhat higher estimates for the SFE. The Gulf region contains the greatest concentration of YSOs and BGPS clumps. Rebull et al. (2011) found 375 YSOs in the 'Gulf of Mexico' cluster whose boundaries closely match and enclose the nearly 800 $M_\odot$ traced by the BGPS. For a median stellar mass of 0.5 $M_\odot$, the implied SFE of the Gulf is about 23% with an uncertainty of at least a factor of two. The Pelican and Atlantic regions in our study are located at the east and west ends of the 'Pelican Cluster' found by Rebull et al. (2011). Our 'Pelican' region contains two dozen Class I and 'flat spectrum' YSOs and an additional two dozen Class II objects. For the same median YSO mass as above, the implied SFE is 18%. The clusters in our 'Atlantic' region only contains four Class I and five 'flat spectrum' sources, consistent with the relatively older age of this region. Adding approximately two dozen Class II sources implies a SFE $\sim$ 7%. However, this may be a severe lower bound as most sources may be Class III or later objects or ones that have lost most of their circumstellar matter.

6. Conclusions

Near-infrared J, H, K_s, and H_2 images of three regions of active star formation associated with 1.1 mm dust clumps surrounding the North America and Pelican (NAP) nebulae are presented. These images reveal many new molecular hydrogen objects (MHOs) which are shocks powered by protostellar outflows propagating into predominantly molecular media. Alignments and source morphology enables some outflows to be identified. The remaining MHOs can not be linked into specific flows or associated with potential driving sources due to indistinct shock orientation or confusion resulting from crowding and the high density of potential driving sources. Comparison with 1.1 mm dust continuum emission from the Bolocam Galactic Plane Survey provides constraints on the evolutionary states of dense molecular clumps.

Summing the masses of the BGPS clumps with radial velocities near $V_{LSR} = 0$ km s^{-1}, and assuming a dust temperature of 20 K gives a BGPS-based mass estimate of 1,120 $M_\odot$ for the mass of dense clumps associated with NGC 7000. The southwestern portion of the Gulf of Mexico region of the NAP contains the most massive and brightest BGPS clump, Gulf SW2.

The 'Pelican' region contains a pair of outflows emerging nearly at right angles from an infrared source embedded in a BGPS clump in the Pelican molecular cloud about a parsec (in projection) from the Pelican ionization front. Their S-shaped symmetries indicate that both outflows are powered by pulsed, precessing jets, likely from an unresolved binary protostar. The Pelican region contains an additional two dozen H_2 shocks emerging from a dozen different low-mass (9 to 60 $M_\odot$) BGPS clumps. Although some MHOs coincide with previously detected HH objects, most do not have visual-wavelength counterparts.

The 'Atlantic' region contains a region of recent star formation with a prominent 8 to 24 μm bubble and a roughly $2'$ (0.3 pc) diameter HII region, G085.07−0.16, with a total radio continuum flux of about 0.5 Jy at 5 GHz. This HII region contains a small IR cluster and a bright source, IRAS 20518+4420, but it may be in a mostly post-star forming state. Only a few MHOs and an outflow mostly traced by 1.644 μm [FeII] emission are found here.

The 'Gulf of Mexico' region contains the largest concentration of outflows, young stars, and the most massive BGPS clumps containing about three-quarters of the dense gas and dust in the entire NAP complex. The region contains well over 300 YSOs in various evolutionary stages, over 100 H_2 shocks grouped into over 50 MHOs, and a candidate massive star forming clump, 'Gulf SW2', which contains the longest outflow detected so far in the NAP. The northeastern portion of the Gulf (the 'Gulf core' region) contains the highest concentration of YSOs and outflows in the NAP with 5% to 10% of the clump surface area covered by H_2 shocks or HH objects. The density of YSOs and outflows is comparable to NGC 1333 in Perseus (Bally et al. 1996). Its ratio of outflow activity to 1.1 mm flux is high. The cloud may be in the process of being disrupted by the energy and momentum deposited by outflow activity.

The Gulf SW2 clump has a mass of about 500 $M_\odot$. However, it only contains a relatively small number of MHOs, including the parsec-scale outflow MHO 3417, which may be powered by a protostar that could be evolving into a massive star. The ratio of YSOs or MHOs to BGPS mass is relatively low. Thus, the Gulf SW2 clump may be in a relatively earlier evolutionary stage than 'Gulf core' (core E and core W in Figure 3). An activity index, formed from the ratio of number of shocks divided by clump mass is proposed as an indicator of the relative evolutionary stage of a clump.

This research was supported by NSF grants # AST 0708403 (The Bolocam Millimeter Wavelength Survey of the Northern Galactic Plane) and # AST 1009847 (Formation of Galactic massive Stars and Star Clusters). BR acknowledges support by the National Aeronautics and Space Administration through the NASA Astrobiology Institute under Cooperative Agreement No. NNA09DA77A issued through the Office of Space Science. GSS is

supported through grants received from NASA. This project made use of ds9 (http://hea-www.harvard.edu/RD/ds9/site/Home.html). This research has made use of the SIMBAD database, operated at CDS, Strasbourg, France. Observations reported here were obtained at the Kitt Peak National Observatory which is operated by the National Optical Astronomy Observatories a nd AURA Inc. with support from the National Science foundation. We thank an anonymous referee for a very thorough reading of the manuscript and useful suggestions which improved the paper and figures.

REFERENCES

Aguirre, J. E. et al. 2011, ApJS, 192, 4

Armond, T., Reipurth, B., Bally, J., & Aspin, C. 2011, A&A, 528, A125

Bally, J. et al. 2010, ApJ, 721, 137

Bally, J., Cunningham, N. J., Moeckel, N., Burton, M. G., Smith, N., Frank, A., & Nordlund, A. 2011, ApJ, 727, 113

Bally, J., Devine, D., & Reipurth, B. 1996, ApJ, 473, L49

Bally, J. & Reipurth, B. 2003, AJ, 126, 893

Bally, J. & Scoville, N. Z. 1980, ApJ, 239, 121

Carrasco-González, C., Anglada, G., Rodríguez, L. F., Torrelles, J. M., Osorio, M., & Girart, J. M. 2008, ApJ, 676, 1073

Comerón, F. & Pasquali, A. 2005, A&A, 430, 541

Daly, P. N. et al. 2008, in Society of Photo-Optical Instrumentation Engineers (SPIE) Conference Series, Vol. 7019, Society of Photo-Optical Instrumentation Engineers (SPIE) Conference Series

Dobashi, K., Bernard, J.-P., Yonekura, Y., & Fukui, Y. 1994, ApJS, 95, 419

Dunham, M. M., Arce, H. G., Bourke, T. L., Chen, X., van Kempen, T. A., & Green, J. D. 2012, ApJ, 755, 157

Elmegreen, B. G. 1998, in Astronomical Society of the Pacific Conference Series, Vol. 148, Origins, ed. C. E. Woodward, J. M. Shull, & H. A. Thronson Jr., 150

Feldt, C. & Wendker, H. J. 1993, A&AS, 100, 287

Ginsburg, A. et al. 2013, ApJS, 208, 14

Glenn, J. et al. 2003, in Proc. SPIE, Vol. 4855, Millimeter and Submillimeter Detectors for Astronomy, 30

Gredel, R. & Reipurth, B. 1994, A&A, 289, L19

Guieu, S. et al. 2009, ApJ, 697, 787

Herbig, G. H. 1958, ApJ, 128, 259

Herbig, G. H. & Bell, K. R. 1988, Third Catalog of Emission-Line Stars of the Orion Population, Lick Observatory Bulletin #1111, Santa Cruz: Lick Observatory, Jun 1988, 90 p

Ishihara, D. et al. 2010, A&A, 514, A1

Kleinmann, S. G., Cutri, R. M., Young, E. T., Low, F. J., & Gillett, F. C. 1986, in Tucson, Univ. of Arizona (1986), 0

Laugalys, V., Straižys, V., Vrba, F. J., Boyle, R. P., Davis Philip, A. G., & Kazlauskas, A. 2006, Baltic Astronomy, 15, 483

Li, Z.-Y. & Nakamura, F. 2006, ApJ, 640, L187

Miller, A. A. et al. 2011, ApJ, 730, 80

Moeckel, N. & Bally, J. 2007a, ApJ, 661, L183

—. 2007b, ApJ, 656, 275

Nakamura, F. & Li, Z.-Y. 2011, ApJ, 740, 36

Planck Collaboration et al. 2011, A&A, 536, A7

Probst, R. G., George, J. R., Daly, P. N., Don, K., & Ellis, M. 2008, in Society of Photo-Optical Instrumentation Engineers (SPIE) Conference Series, Vol. 7014, Society of Photo-Optical Instrumentation Engineers (SPIE) Conference Series

Rebull, L. M. et al. 2011, ApJS, 193, 25

Reipurth, B. 2000, AJ, 120, 3177

Reipurth, B., Mikkola, S., Connelley, M., & Valtonen, M. 2010, ApJ, 725, L56

Reipurth, B. & Schneider, N. 2008, Star Formation and Young Clusters in Cygnus, Handbook of Star Forming Regions, Volume I, ed. Bo Reipurth, PASP Monograph 4, p. 36, ed. B. Reipurth, 36

Rosolowsky, E. et al. 2010, ApJS, 188, 123

Schlingman, W. M. et al. 2011, ApJS, 195, 14

Semkov, E. H., Peneva, S. P., Munari, U., Milani, A., & Valisa, P. 2010, A&A, 523, L3

Semkov, E. H. et al. 2012, A&A, 542, A43

Shirley, Y. L. et al. 2013, ApJS, 209, 2

Straižys, V. & Laugalys, V. 2008, Baltic Astronomy, 17, 143

Toujima, H., Nagayama, T., Omodaka, T., Handa, T., Koyama, Y., & Kobayashi, H. 2011, PASJ, 63, 1259

Usuda, T., Sugai, H., Kawabata, H., Inoue, M. Y., Kataza, H., & Tanaka, M. 1996, ApJ, 464, 818

Welin, G. 1973, A&AS, 9, 183

Zhang, S. B., Yang, J., Xu, Y., Pandian, J. D., Menten, K. M., & Henkel, C. 2011, ApJS, 193, 10

This preprint was prepared with the AAS LaTeX macros v5.2.

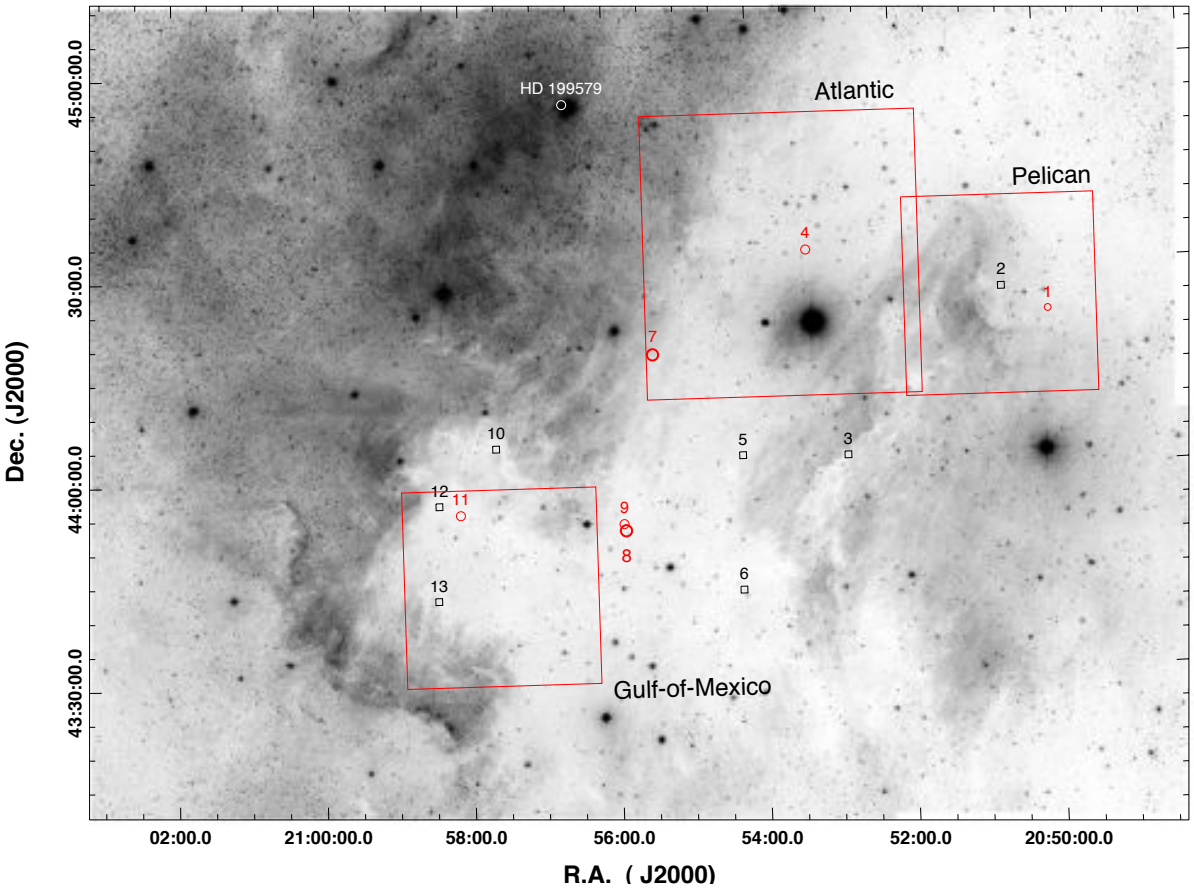

Fig. 1.— A wide-field image of the NGC 7000 region showing the regions observed in this study taken from the digitized red sensitive (E) plates of the Palomar Sky Survey. The locations of stars identified by Straizys & Laugalys (2008) are indicated: Red circles mark stars they classified as spectral type OB. The two circles with larger radii (#7 and #8) indicate the two most massive O5 stars. Squares indicate massive stars thought to be AGB stars based on photometry. The large red boxes indicate the fields imaged with NEWFIRM.

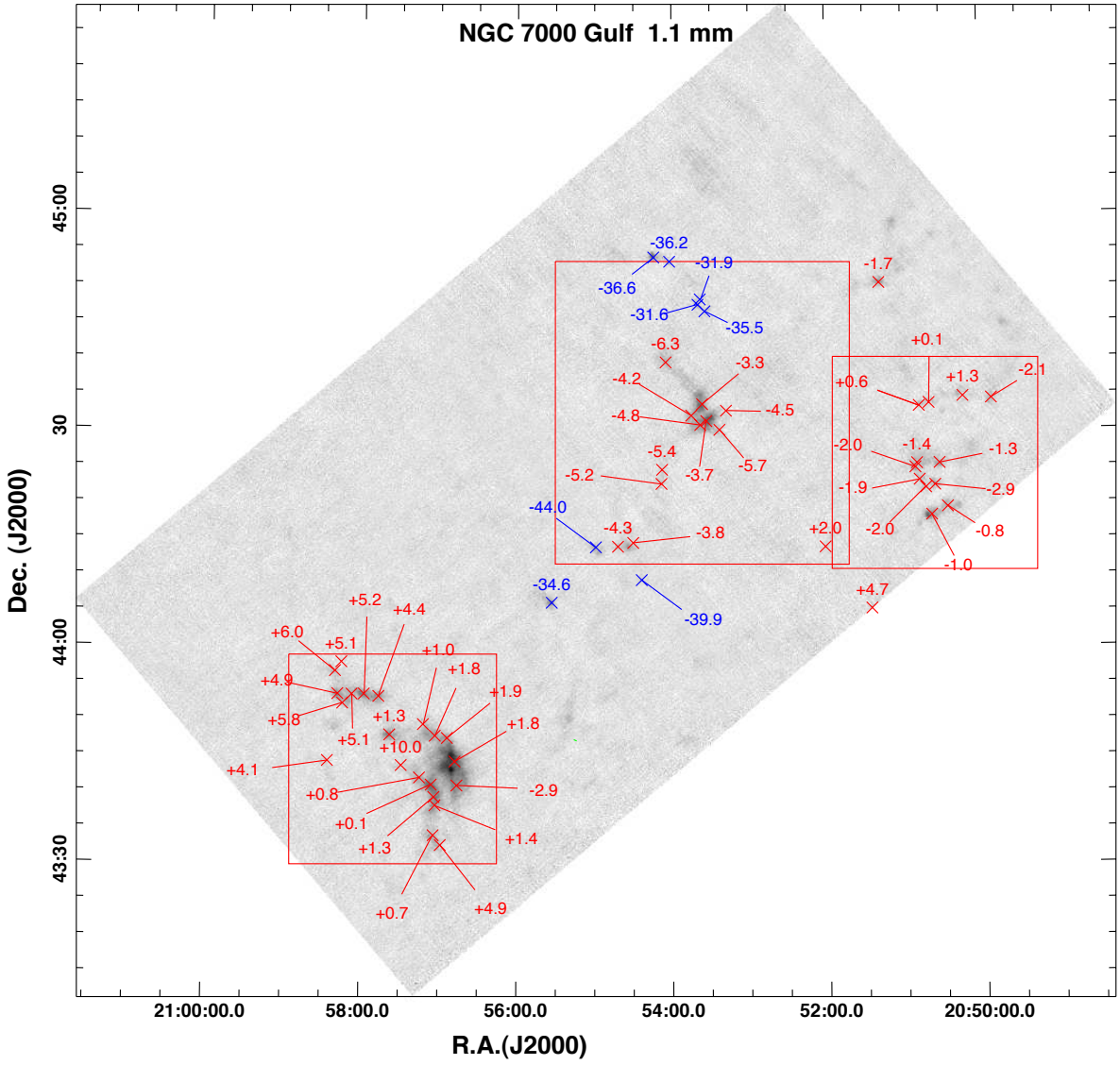

Fig. 2.— A 1.1 mm dust continuum image showing clumps in the NGC 7000 region taken from the Bolocam Galactic Plane Survey (BGPS) in Galactic coordinates. Locations where the J = 3-2 transition of HCO^+ were detected are marked with an X. The numbers next to each X indicate the LSR velocity determined from a Gaussian fit to the spectrum. Values with $-10.0 < V_{LSR} < +10.0$ are shown in red; values with $V_{LSR} < -10.0$ are shown in blue. The large red boxes indicate the fields imaged with NEWFIRM as in Figure 1.

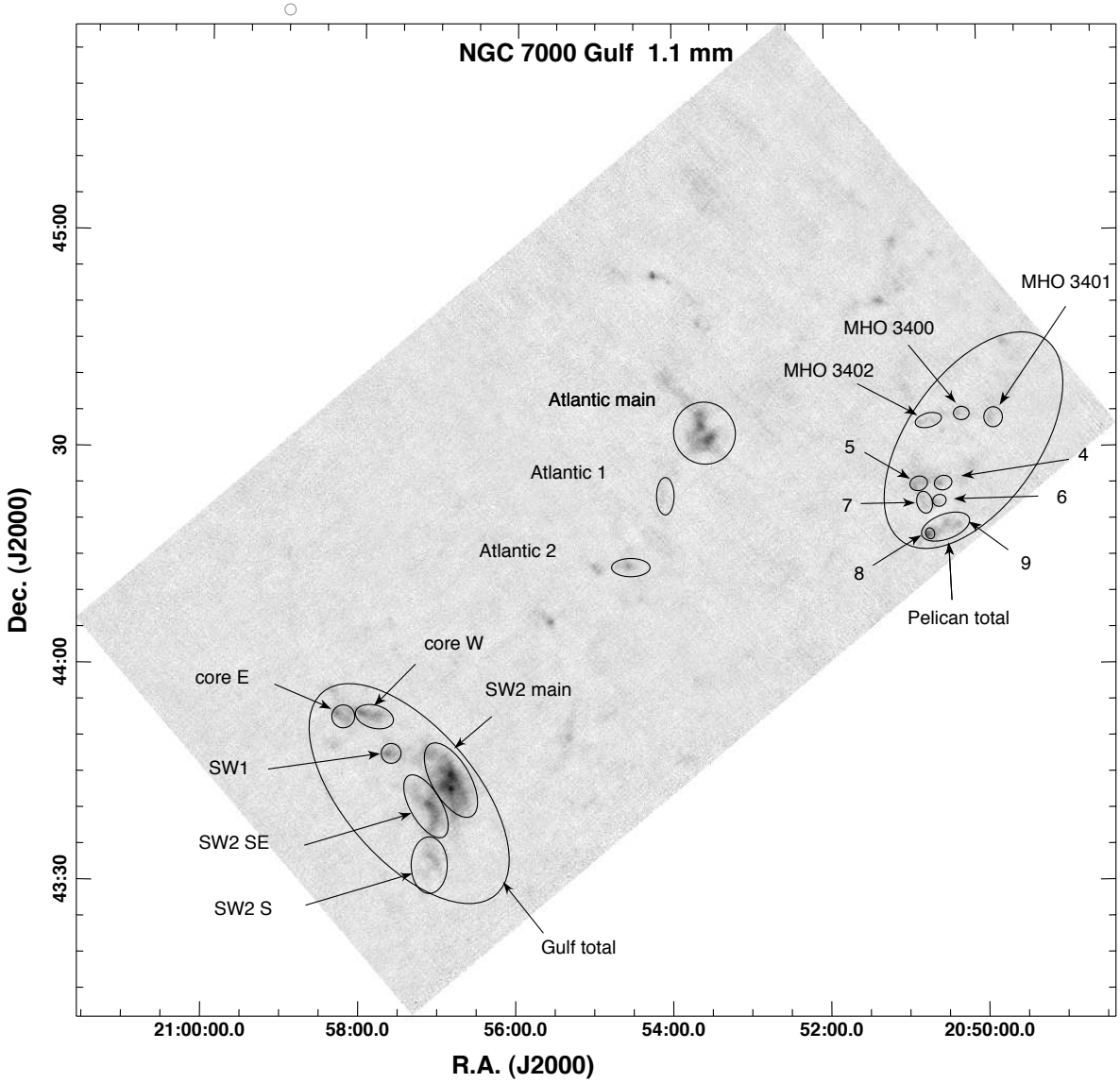

Fig. 3.— The 1.1 mm BGPS image showing the regions inside which masses listed in Table 4 were evaluated. Masses were calculated only for objects having radial velocities indicating an association with NGC 7000 (the NAP) and thought to lie at a distance of about 550 pc.

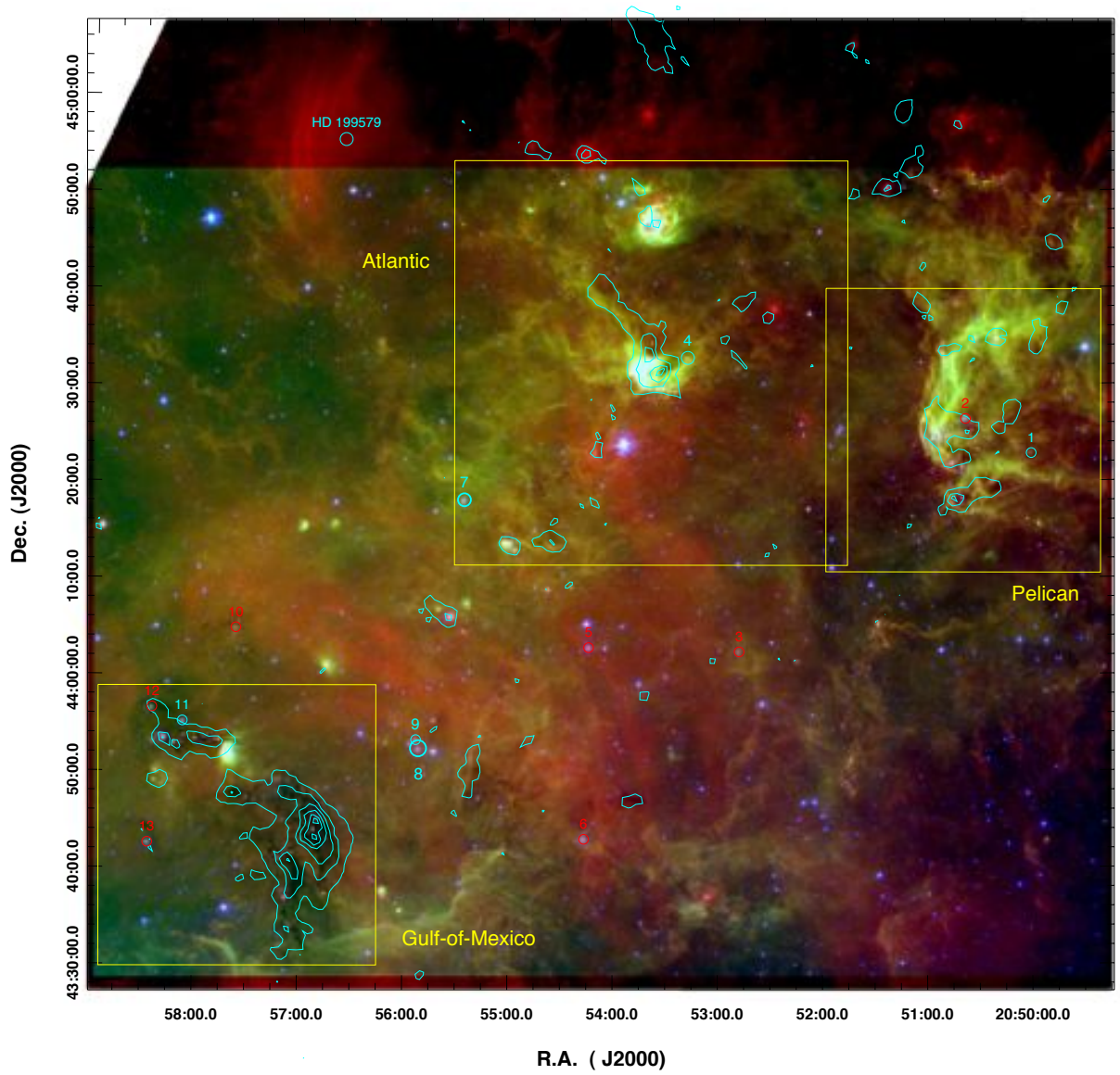

Fig. 4.— A Spitzer Space Telescope image showing emission at 24 μm (red), 8.0 μm (green), and 4.5 μm (blue). BGPS contours (Figure 1) are superimposed. Stars from Straizys & Laugalys (2008) are indicated along with the NEWFIRM fields of view. Those marked in cyan are OB stars. Those marked in red are post main-sequence massive stars.

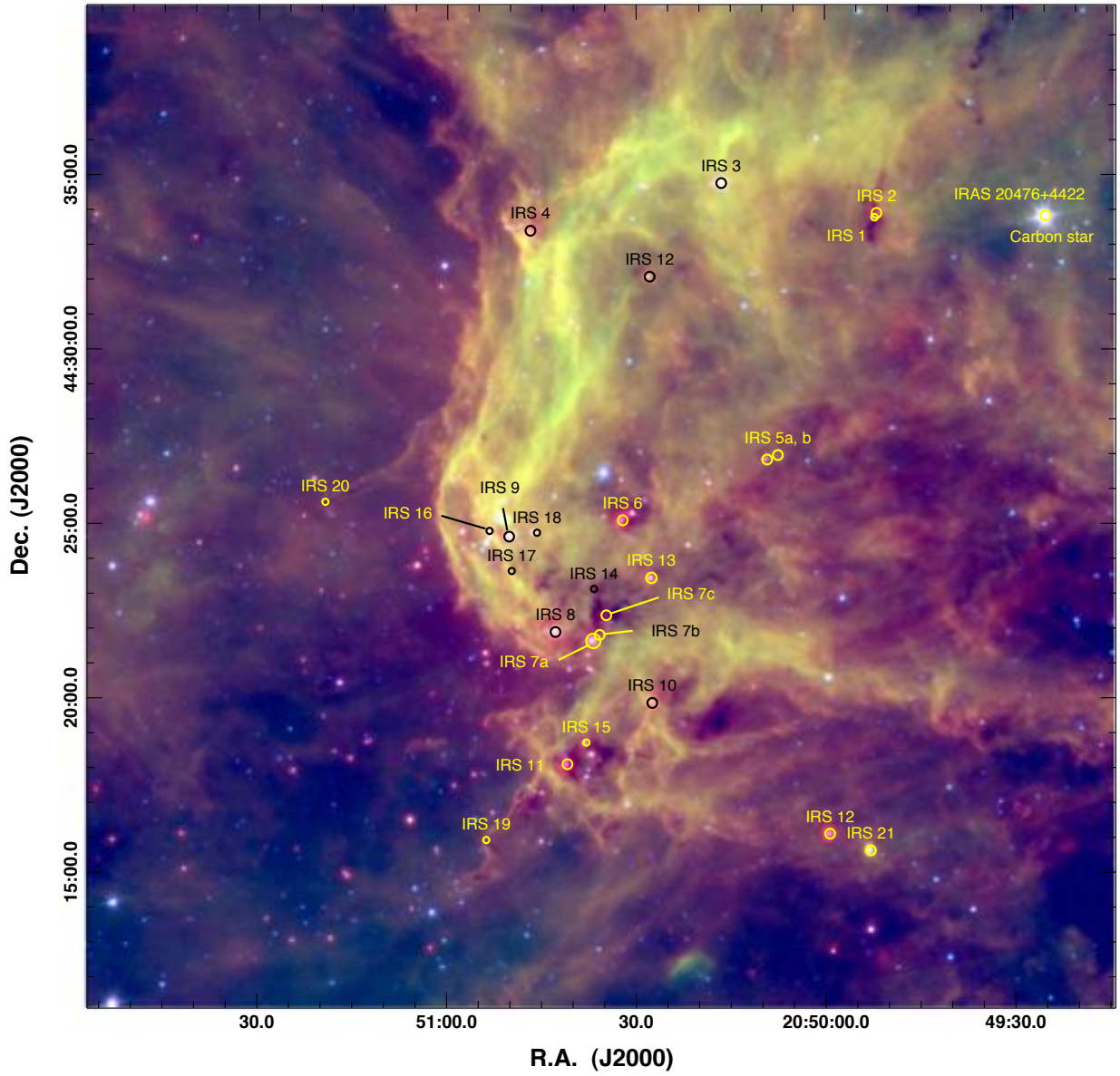

Fig. 5.— A color composite image showing 4.5 (blue), 8 (green), and 24 μm (red) emission in the Pelican Region with the locations of 70 μm sources shown with yellow circles (or black where the background is bright). Numbers correspond to the entries in Table 1 and the text.

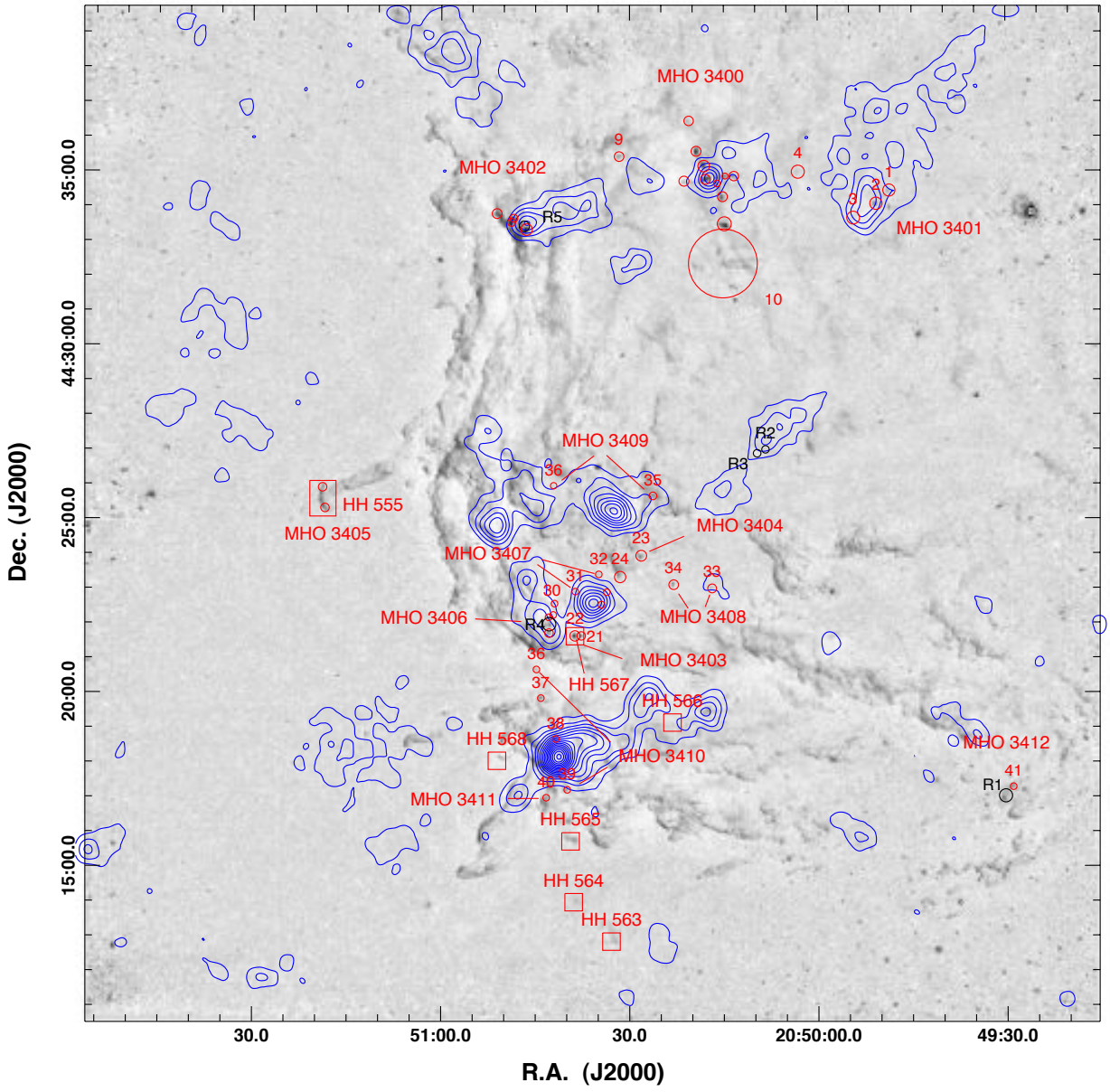

Fig. 6.— A continuum-subtracted 2.12 μm H_2 image showing the Pelican Nebula region with contours showing the 1.1 mm dust continuum emission contours from the Bolocam Galactic Plane Survey (BGPS). Contour levels are shown at intervals of 0.05 Jy from 0.05 Jy to 1.0 Jy per 33″ beam. Circles show the locations of shock-excited molecular hydrogen objects (MHOs). Small red numbers above some red circles correspond to the Table 1 entries for the Pelican region. Black circles mark near-IR reflection nebulae. The locations of previously discovered Herbig-Haro objects (Bally & Reipurth 2003) are indicated by squares.

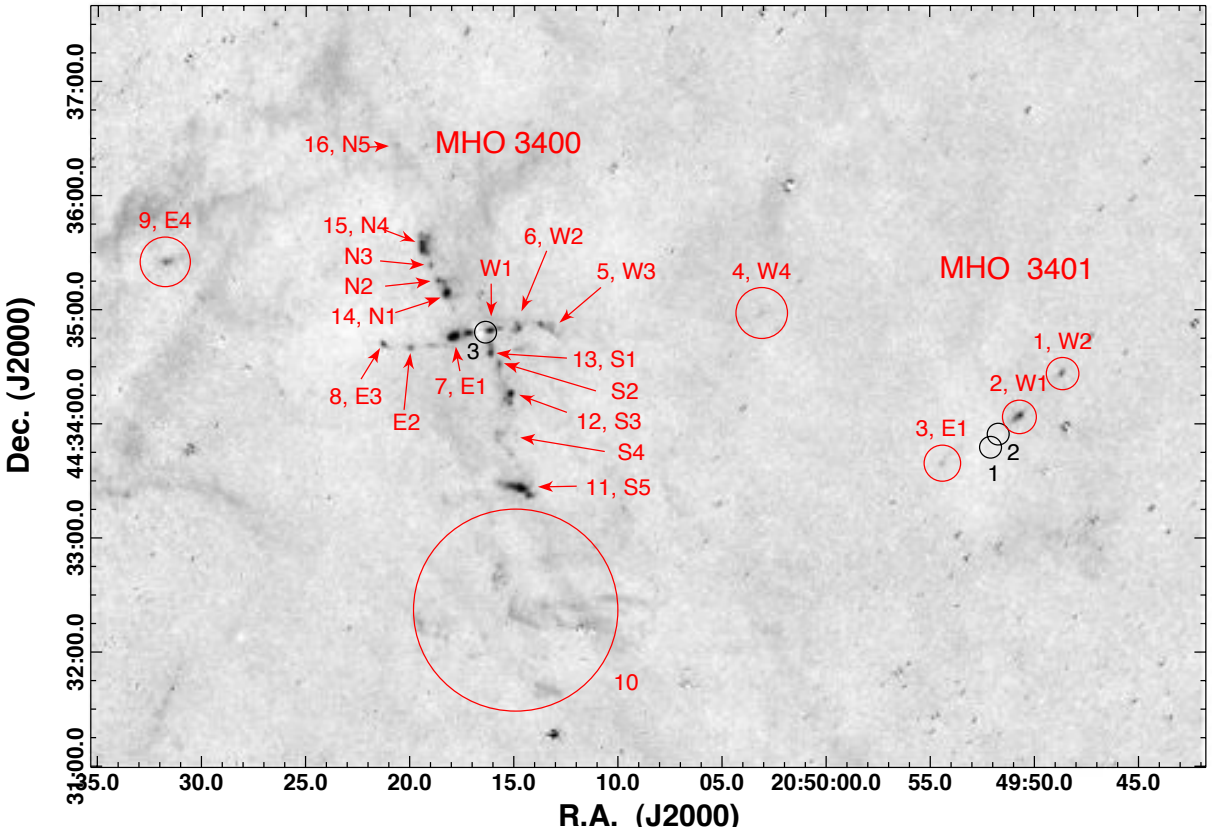

Fig. 7.— A continuum subtracted H_2 image showing the quadrupolar outflow MHO 3400 embedded in the northwest clump in the Pelican Nebula (left) and the outflow MHO 3401 emerging from a protostar embedded in a BGPS clump. The large circle encloses a feature which may be a shock along the MHO 3401 axis or a fluorescent edge. Black circles mark locations of the Spitzer-detected IR sources discussed in the text. The source labeled as 2 (IRS 2 in Table 1) is more embedded and likely the source of MHO 3401. Source 3 (listed as IRS 3 in Table 1) at the center of MHO 3400 is IRAS 20485+4423.

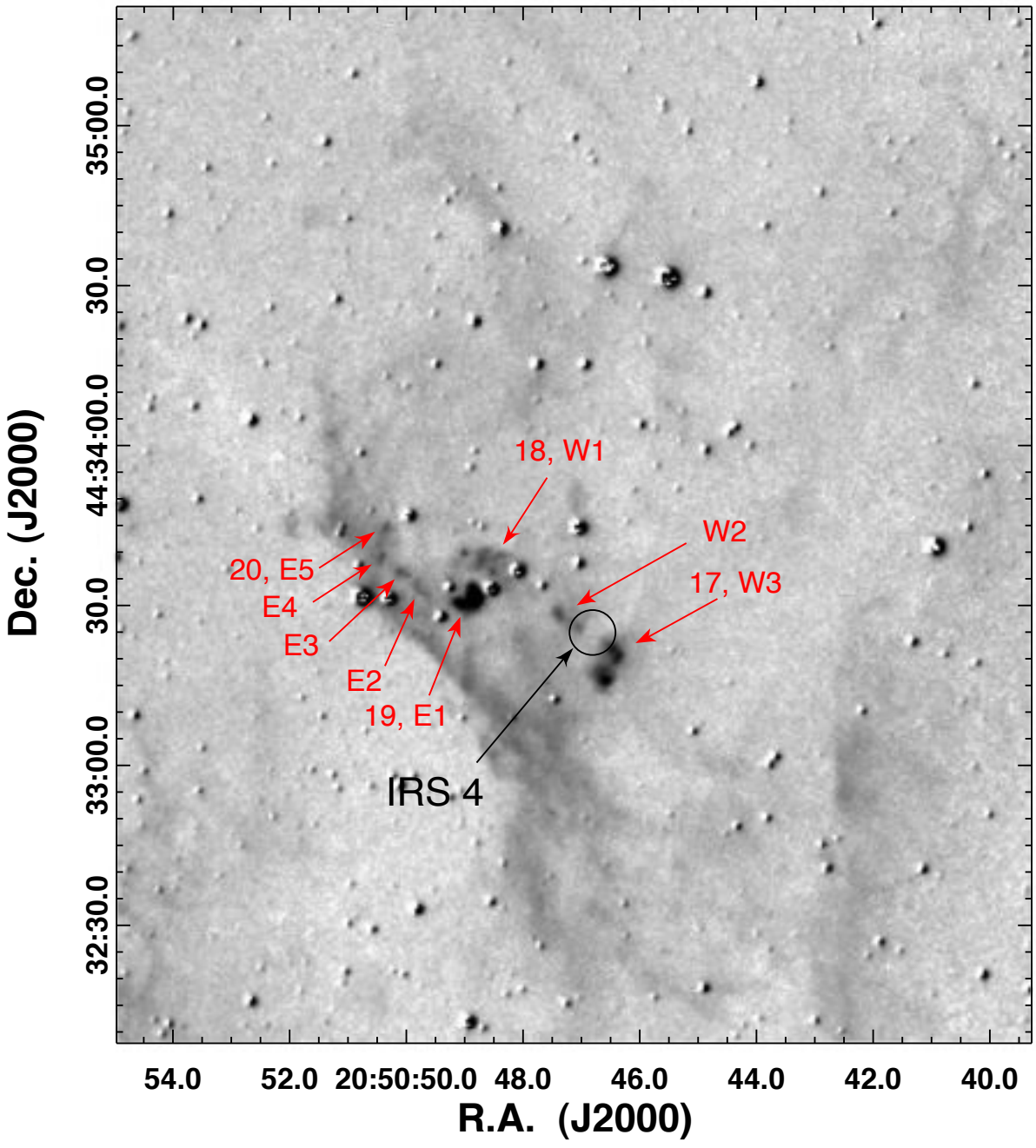

Fig. 8.— A continuum subtracted 2.12 μm H_2 image showing the field around MHO 3402 at the ionization front in the Pelican region. As discussed in the text the knots preceded by 'W' (west) and 'E' (east) may trace at least two distinct outflows from YSOs in this small aggregate. The source IRS 4 corresponds to the 8 to 70 μm object listed in Table 1.

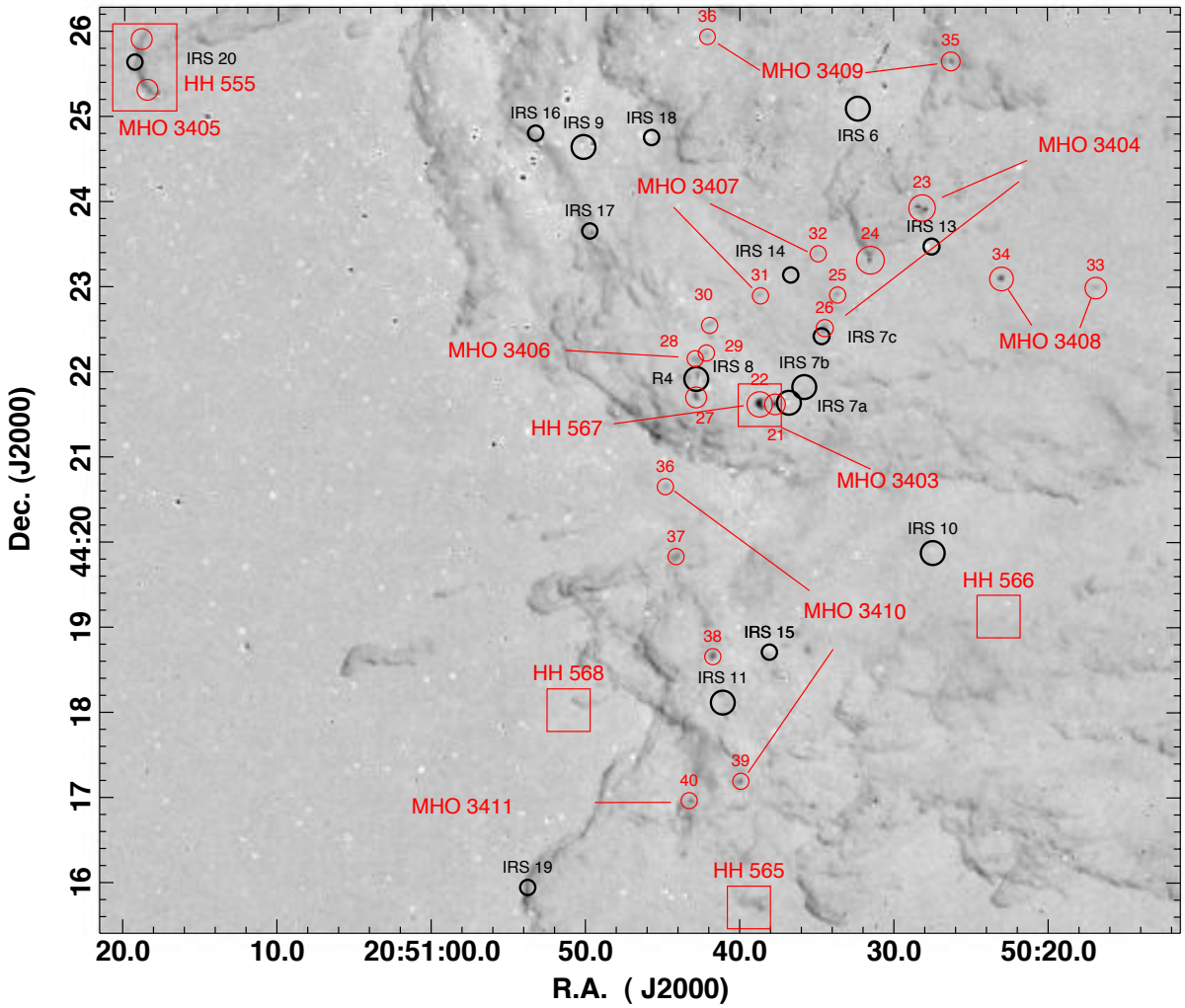

Fig. 9.— A 2.12 μm continuum subtracted H_2 image showing the cluster of MHOs and highly embedded YSOs in the southeast portion of the Pelican region. The brightest, highly embedded Spitzer detected YSOs are shown: black circles are 70 μm sources.

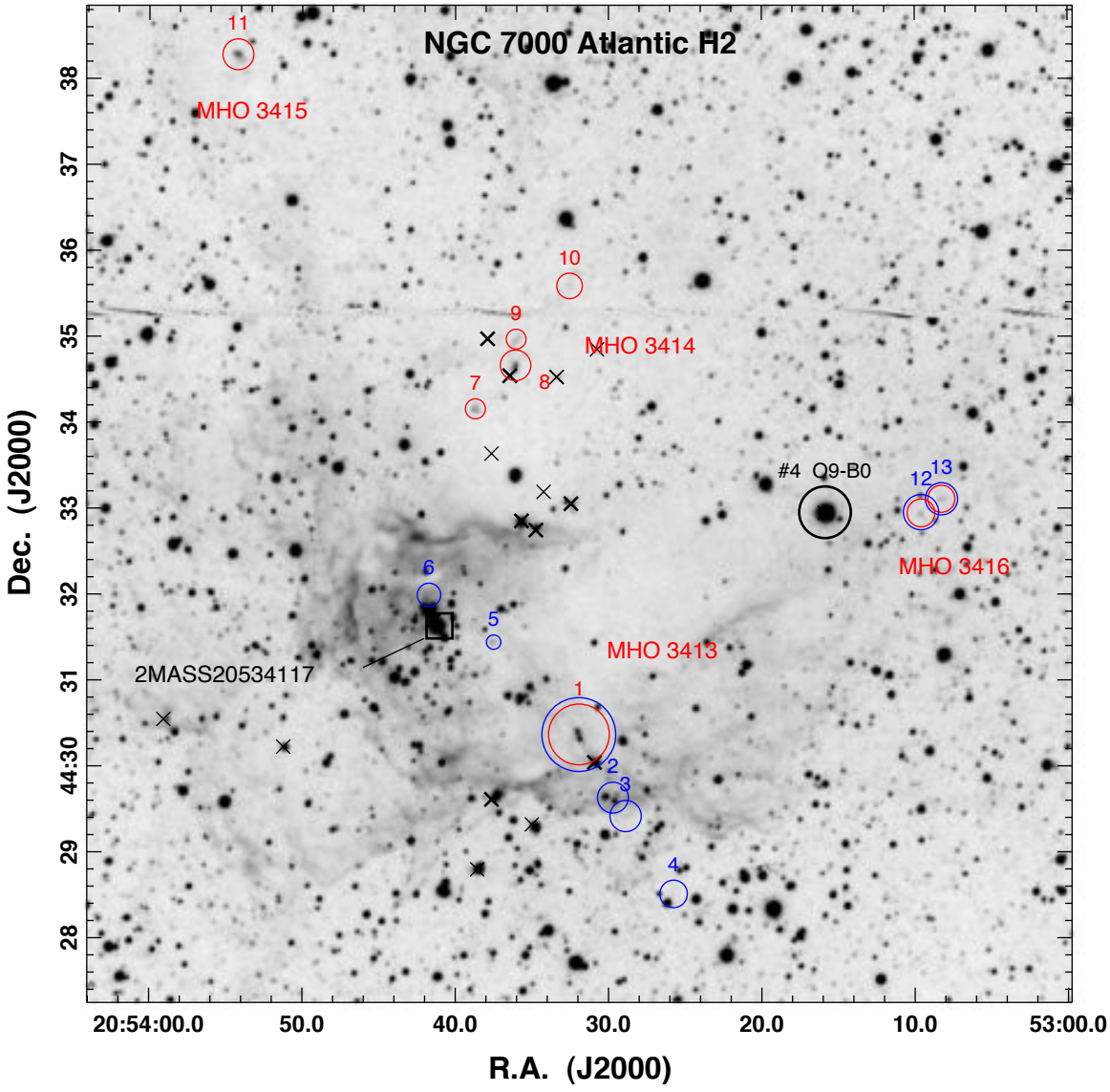

Fig. 10.— A 2.12 μm H_2 image showing the field around cluster and HII region G085.06−0.16 in the "Atlantic core" region. The brightest 2 μm source, 2MASS 20534117+44311378 discussed in the text (only the digits before the '+' are given), is marked. Red circles show candidate H_2 shocks; blue circles are the [FeII] knots shown in Figure 11. The corresponding K_s image was plagued by clouds and could not be used for continuum subtraction. The black circle shows Straizys and Laugalys (2008) star #4, suspected to be an O9 or B0 massive star. The black crosses mark 24 μm sources. The brighter ones have darker marks. The horizontal band near the top is a cosmetic defect.

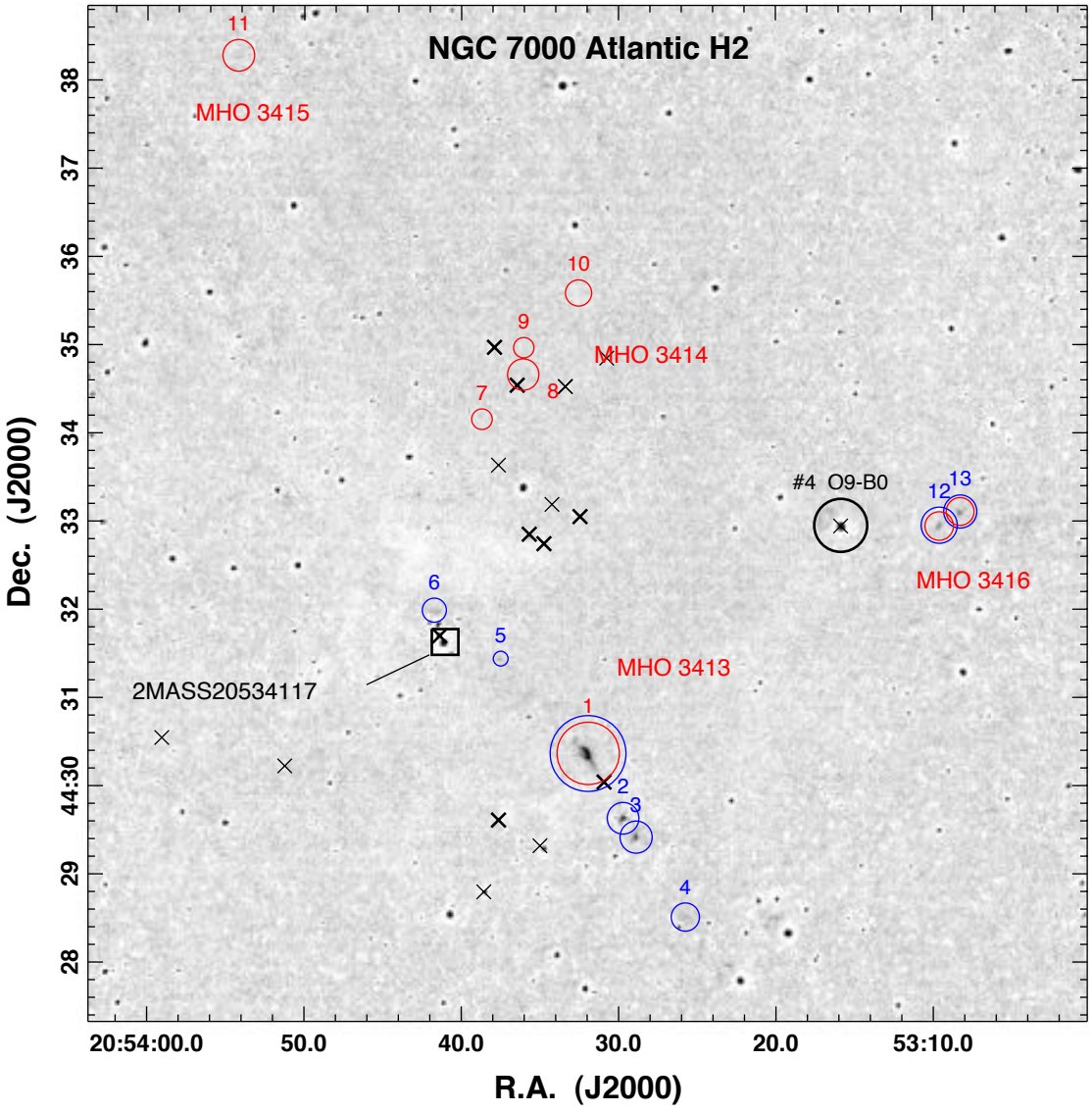

Fig. 11.— A continuum subtracted 1.64 μm [FeII] image showing the jet near the 2MASS source (black square) in the "Atlantic gulf " region. Red circles show candidate H_2 shocks; blue circles show the [FeII] knots. The black circle shows Straizys and Laugalys (2008) star #4, suspected to be an O9 or B0 massive star. The black crosses mark 24 μm sources. The brighter ones have darker marks.

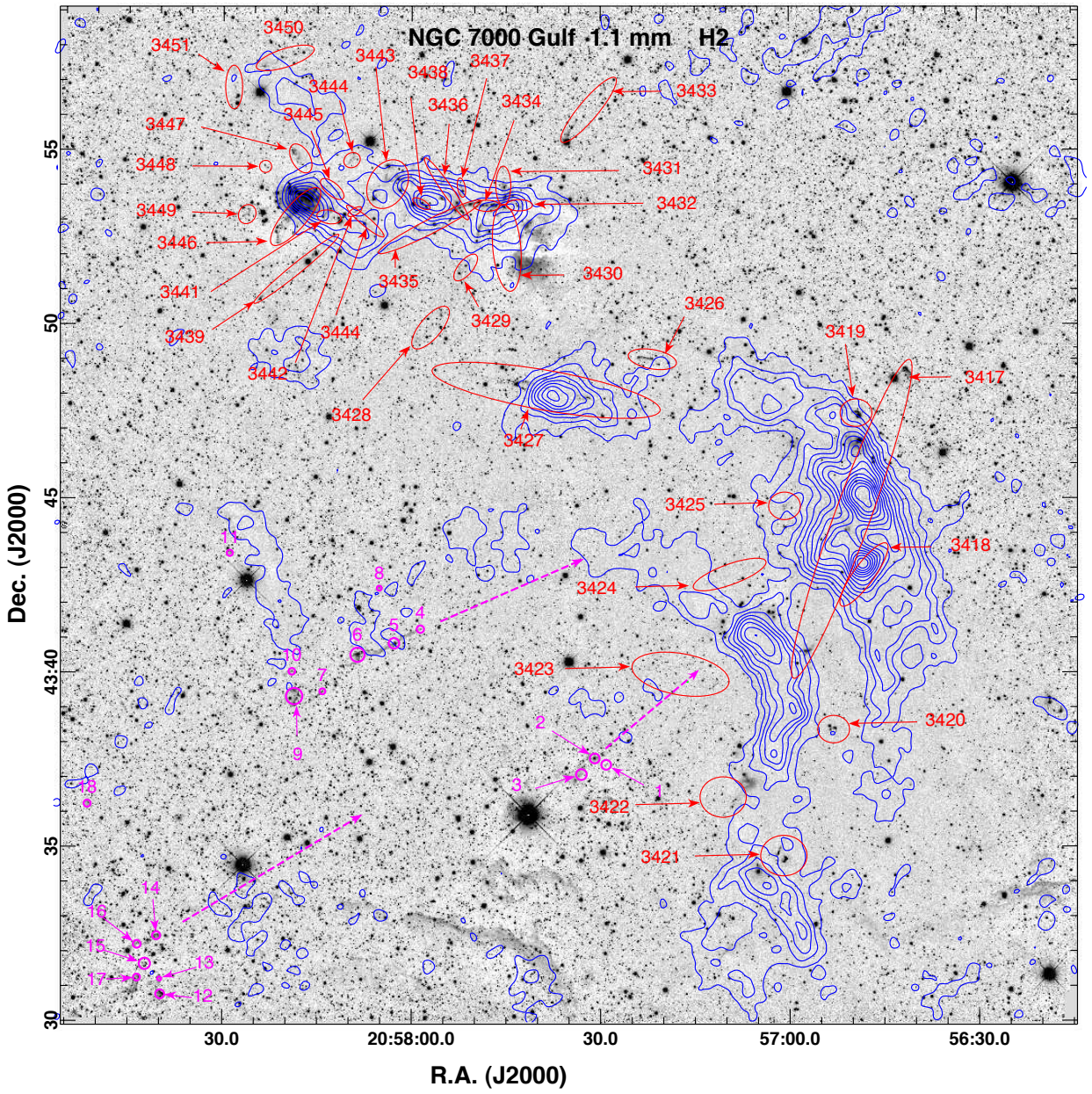

Fig. 12.— A 2.12 μm H_2 image showing the Gulf of Mexico field. Red ovals mark MHOs listed in Table 3. The cyan circles in the lower left mark cometary clouds traced by fluorescent H_2 emission from cloud edges listed in Table 3 with a letter 'C' in the Comments column. The mean orientations of the three groups of cometary clouds are indicated by the dashed arrows. Figures 20, 21, and 22 show close-up views of these objects These elongated clouds point to one of the exciting stars of the NAP, star #8 (the spectral type O5 Comerón & Pasquali star) . Contours show $\lambda = 1.1$ mm BGPS dust continuum emission with levels at 0.19, 0.26, 0.34, 0.41, 0.48, 0.55, 0.63, 0.70, 0.78, 0.85, 0, 93, 1.0, and 1.07 Jy/beam.

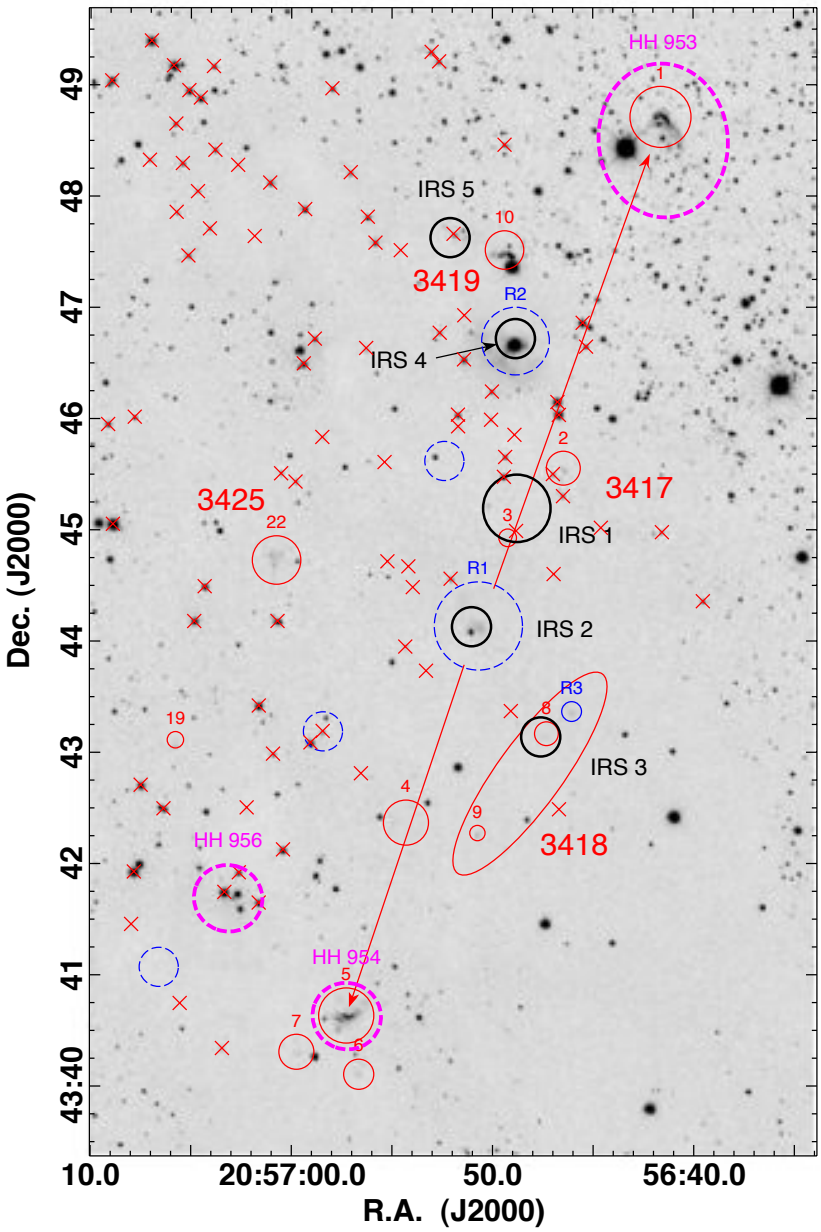

Fig. 13.— An H_2 image showing details in the Gulf SW2 region containing the large molecular hydrogen outflow MHO 3417. Thin circles and ovals (red) mark MHOs with numbers listed in Table 3. Crosses (red 'x' symbols in the electronic version) mark locations of YSOs identified in Guieu et al. (2009). Thin dashed circles (blue) marked with the letter 'R' followed by a number mark 2 μm reflection nebulae indicated in Table 3. Thick black solid circles mark 70 μm sources. Thick dotted ovals and circles mark locations of HH objects.

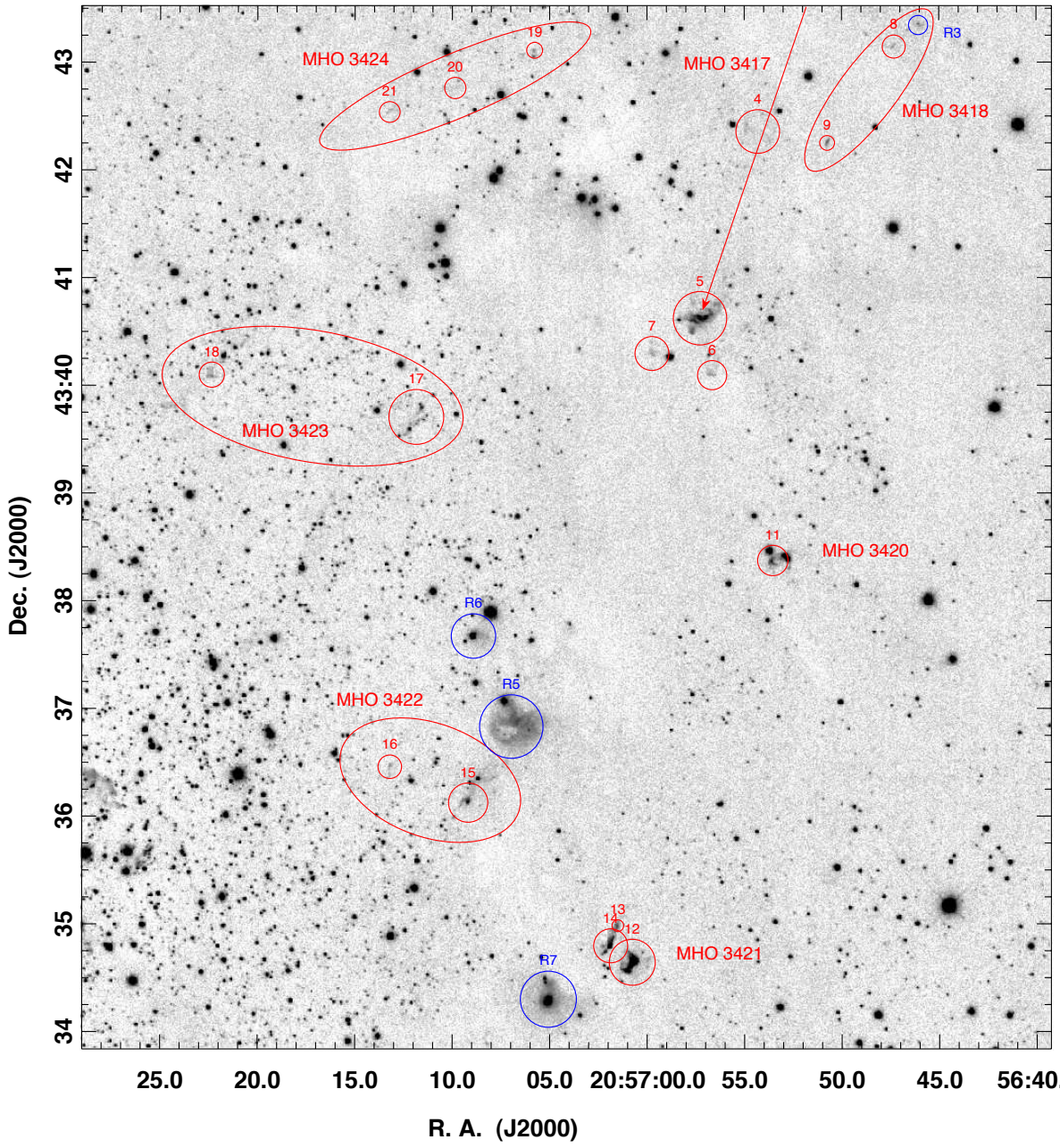

Fig. 14.— An H_2 image showing the field containing 'Gulf SW2 SE' and 'SW2 S' and MHO 3420 through MHO 3424.

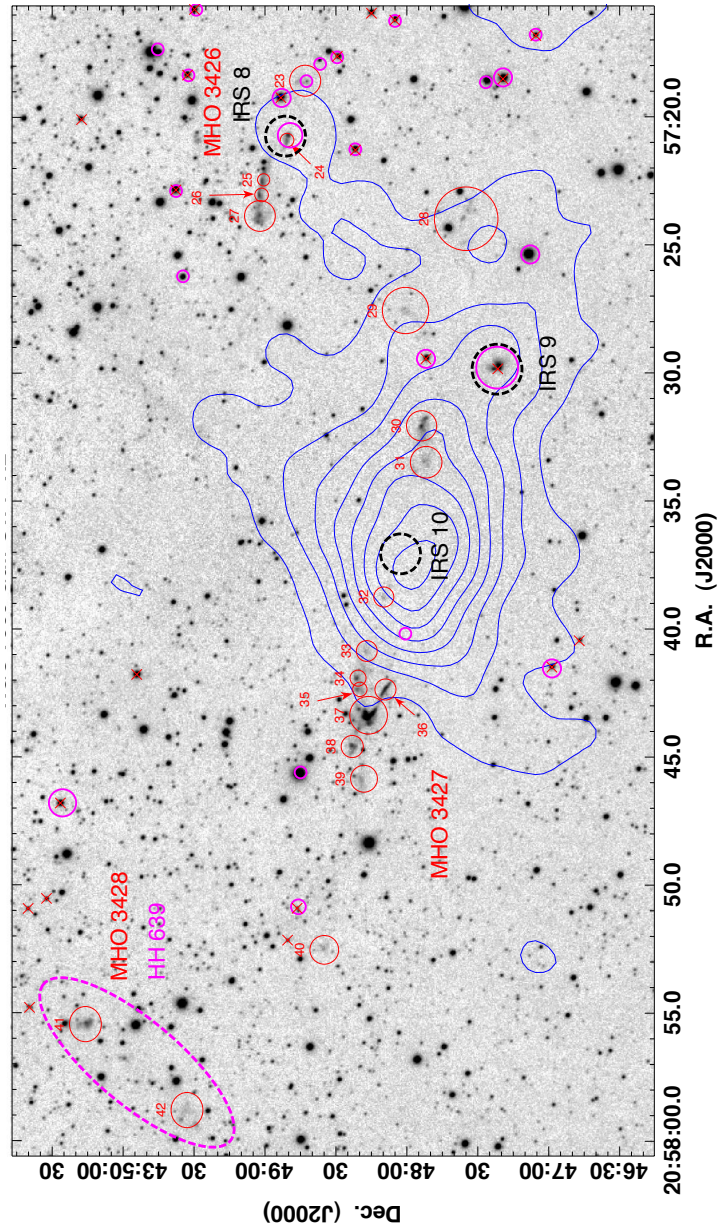

Fig. 15.— Molecular hydrogen outflows emerging from the Gulf SW 1 core (IRDC G84.963-1.117) in NGC 7000. Thin red circles with numbers mark MHOs located in the Gulf of Mexico region (Table 3). Bold dashed circles mark Spitzer 70 μm sources. Bold solid circles (magenta in electronic version) mark Spitzer 24 μm sources; 'crosses ('x's) mark YSOs identified by Guieu et al. (2009). The source of the large east-west H_2 outflow, MHO 3427, may be a Class 0 protostar visible only at a wavelength of 70 μm and marked by the black circle above IRS 10 in the image. Contours (blue) show the 1.1 mm dust continuum emission detected by the Bolocam Galactic Plane Survey. Contour levels are shown at intervals of 0.074 Jy from 0.04 Jy to 1.7 Jy per 33″ beam.

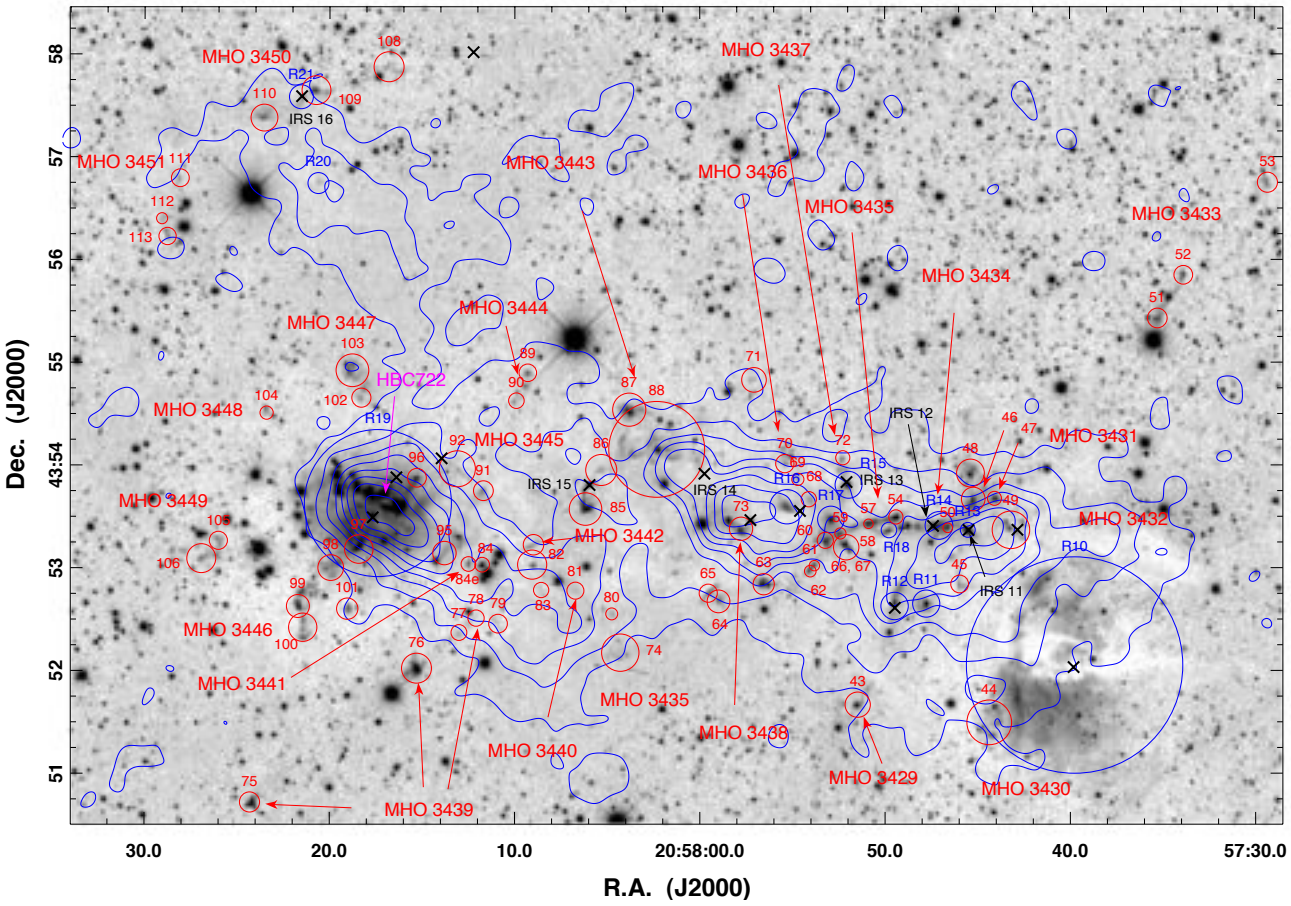

Fig. 16.— Molecular hydrogen objects (red in the electronic version of the paper) and reflection nebulae (blue circles in the electronic version of the paper) located in the Gulf 'core E' and 'core W' regions. The intensity is displayed with a log stretch. The numbers correspond to the entries in Table 3. Reflection nebulae are preceded by a letter 'R'. 70 μm sources are marked with an 'x'. Contours trace the 1.1 mm dust continuum emission. Circles indicate the locations of MHOs and reflection nebulae as listed in Table 3. Some objects listed in Table 3 such as knots 55 and 56 that lie between 54 and 57 are not marked to avoid confusion from overlapping symbols. Knot 82n in Table 3 is marked as MHO 3442.

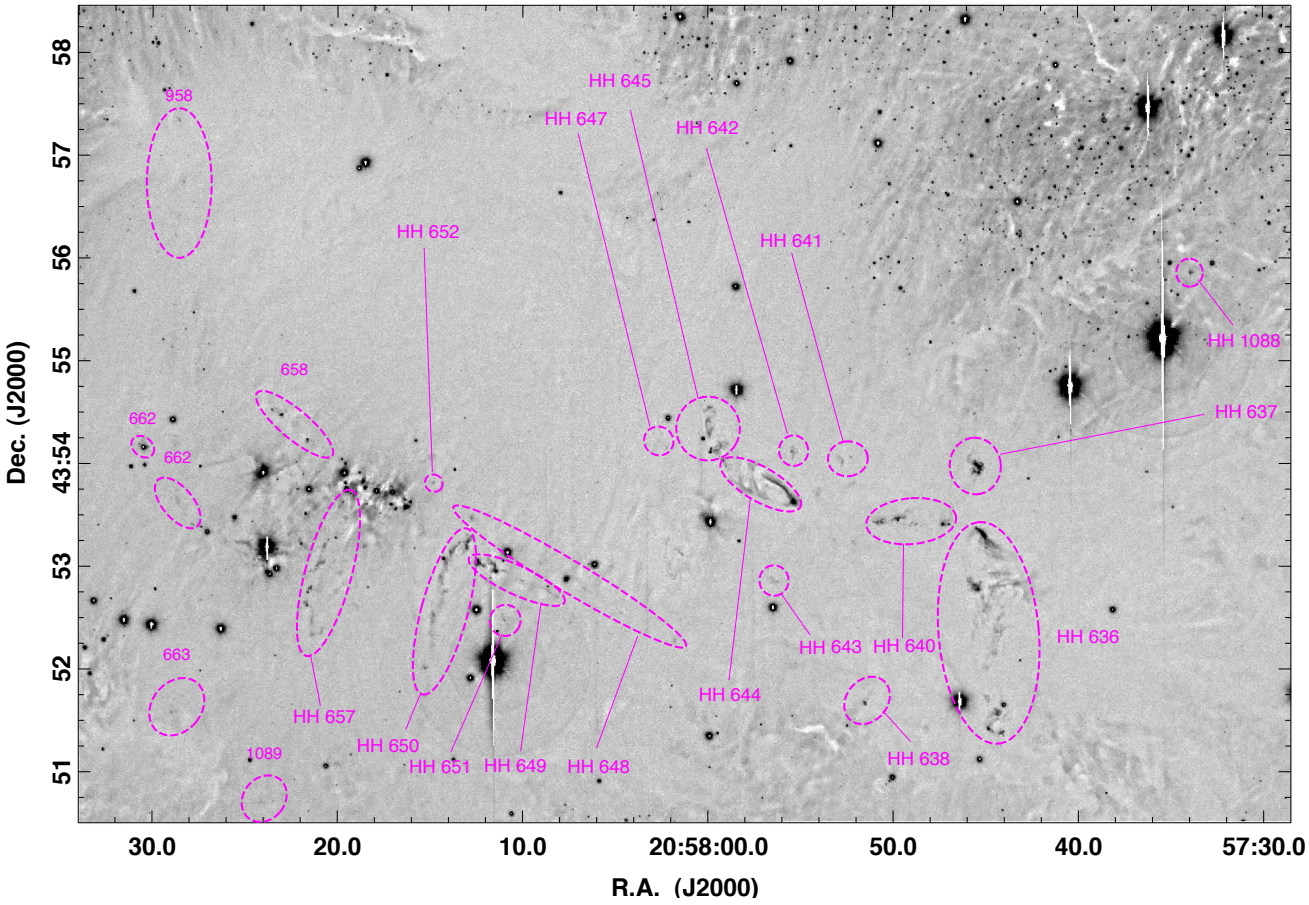

Fig. 17.— A greyscale image showing λ 0.6717/0.6731 μm [SII] emission. The image was processed with a filtering algorithm to remove large-scale, large-amplitude background variations. First, the image is convolved with a 21-pixel top-hat function. Second, the convolved image is scaled by a numerical factor of 0.9 to create a mask image. Third, the mask image is subtracted from the original image. The region shown is the same as Figure 16.

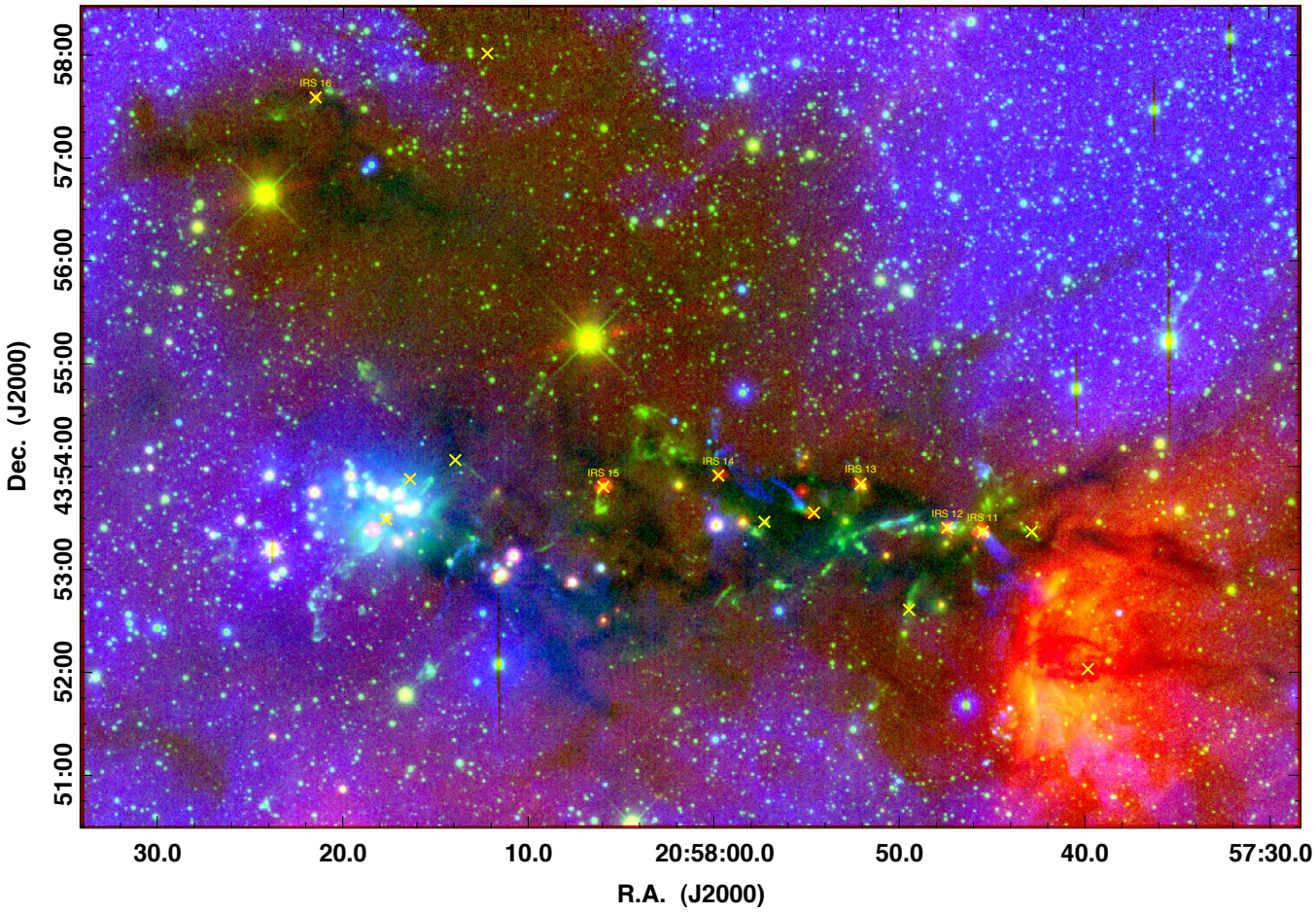

Fig. 18.— (Electronic version only) A color image combining NEWFIRM λ 2.12 μm H_2 emission (green), Subaru 0.67 μm [SII] (blue), and Spitzer 8 μm (red). Yellow 'X' symbols mark locations of highly embedded 70 μm sources. The two bright yellow sources are red giant stars unrelated to the NAP. The region shown is the same as Figure 16.

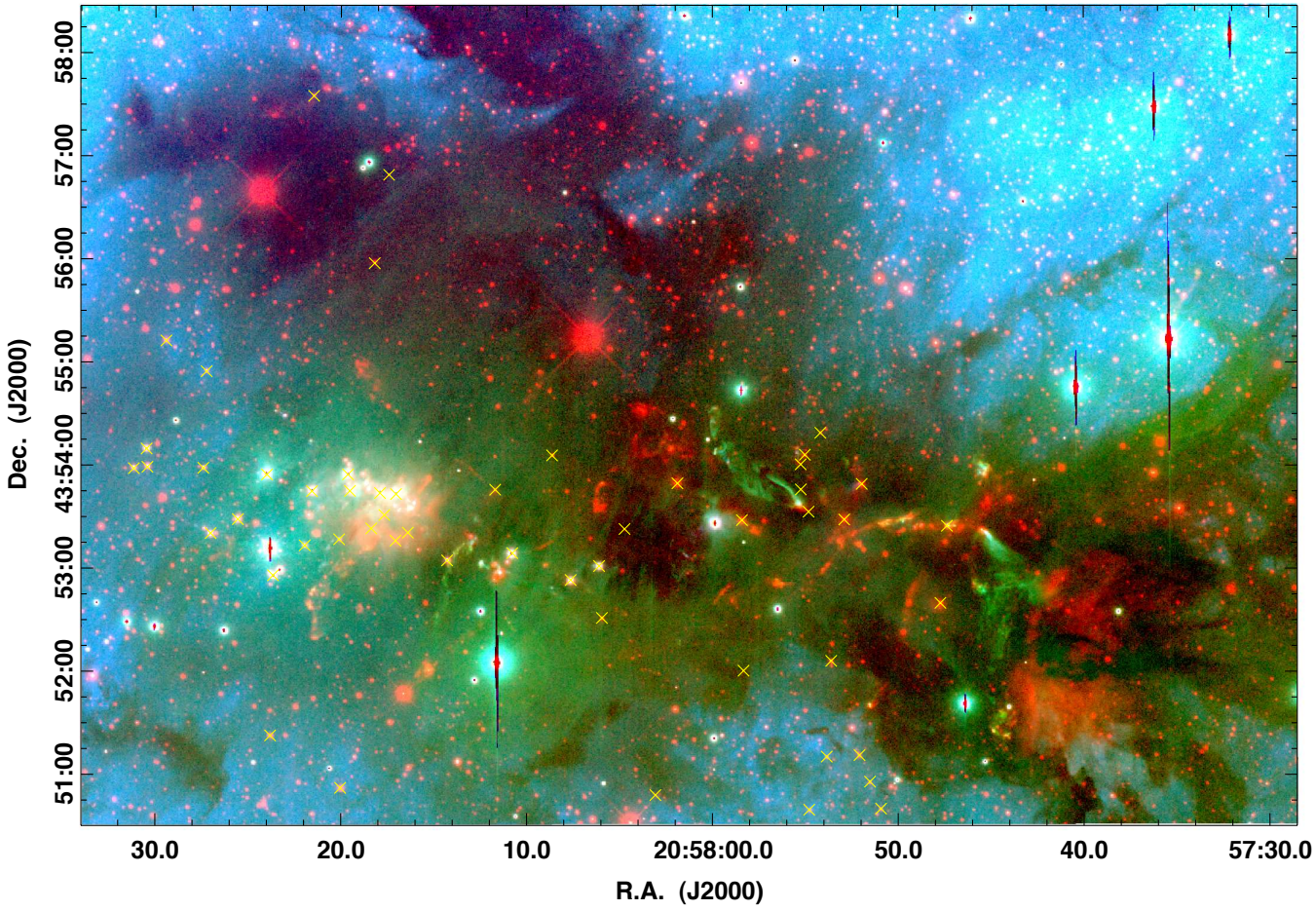

Fig. 19.— (Electronic version only) A color image showing 0.6563 μm Hα (blue), $\lambda\lambda$ 0.6717/0.6731 μm [SII] (green), and λ 2.12 μm H_2 emission (red). Crosses mark YSOs identified by Guieu et al. (2009). The region shown is the same as Figure 16.

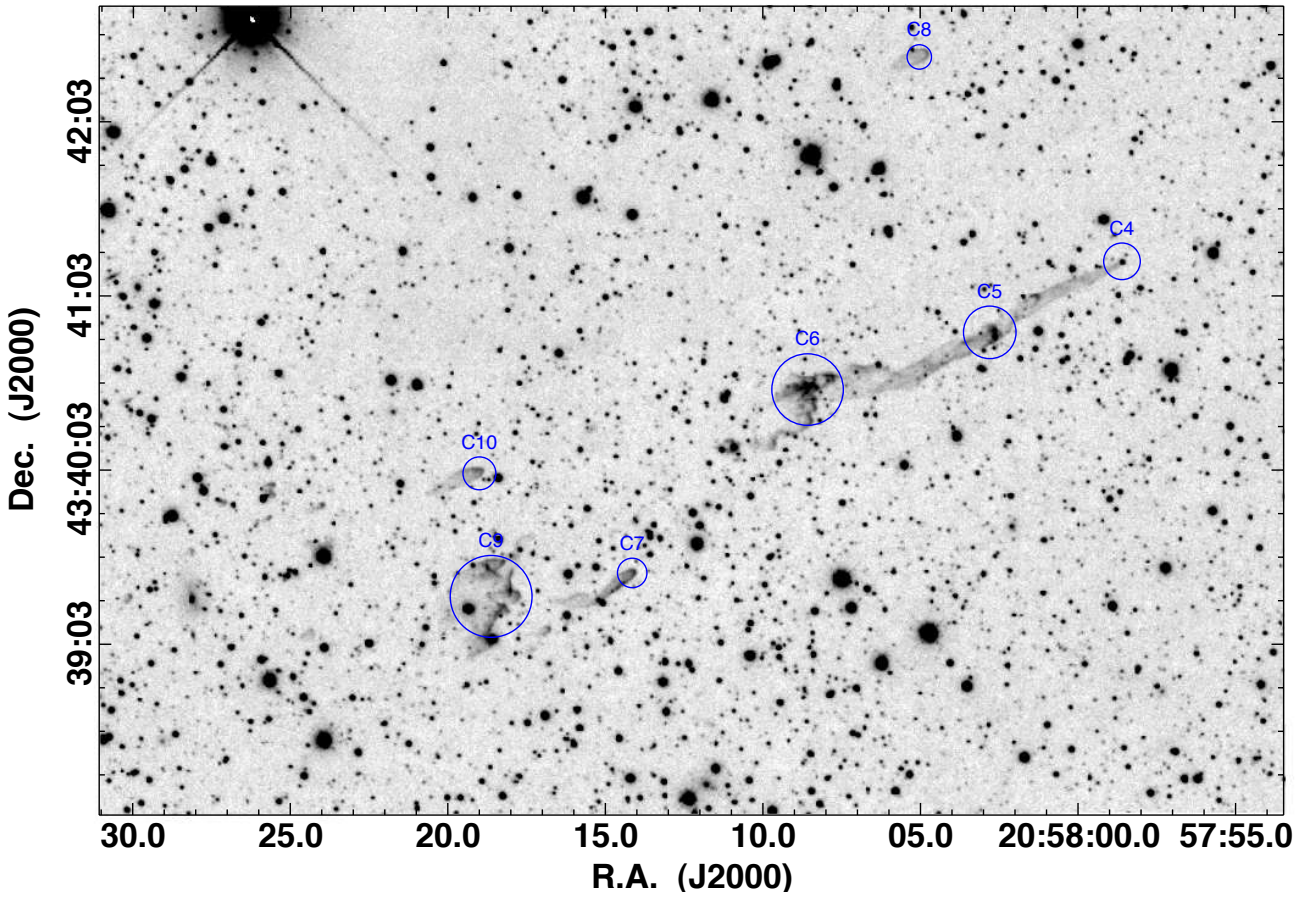

Fig. 20.— 2.12 μm image showing several cometary clouds (C4 through C10) southeast of the Gulf of Mexico.

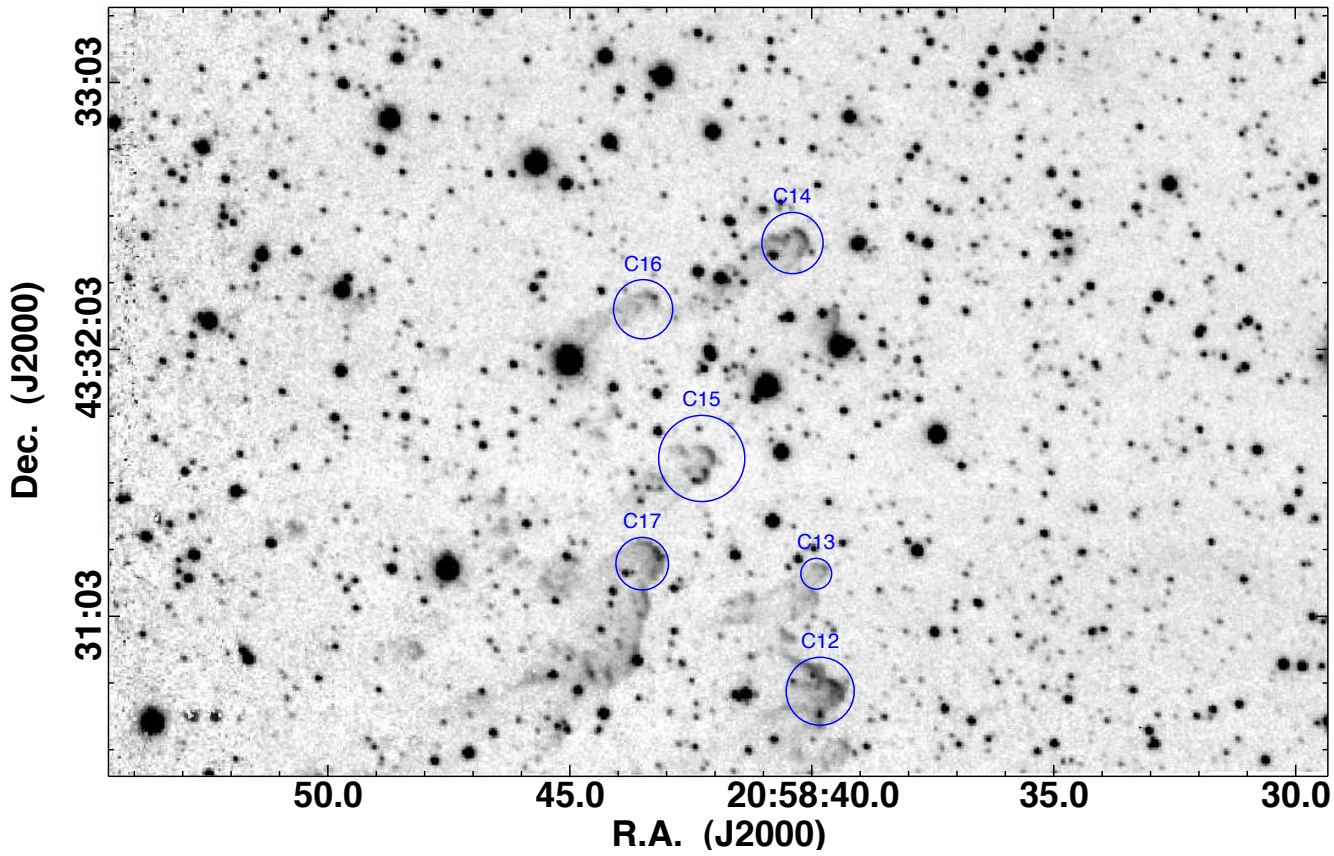

Fig. 21.— 2.12 μm image showing several cometary clouds (C12 through C17) southeast of the Gulf of Mexico.

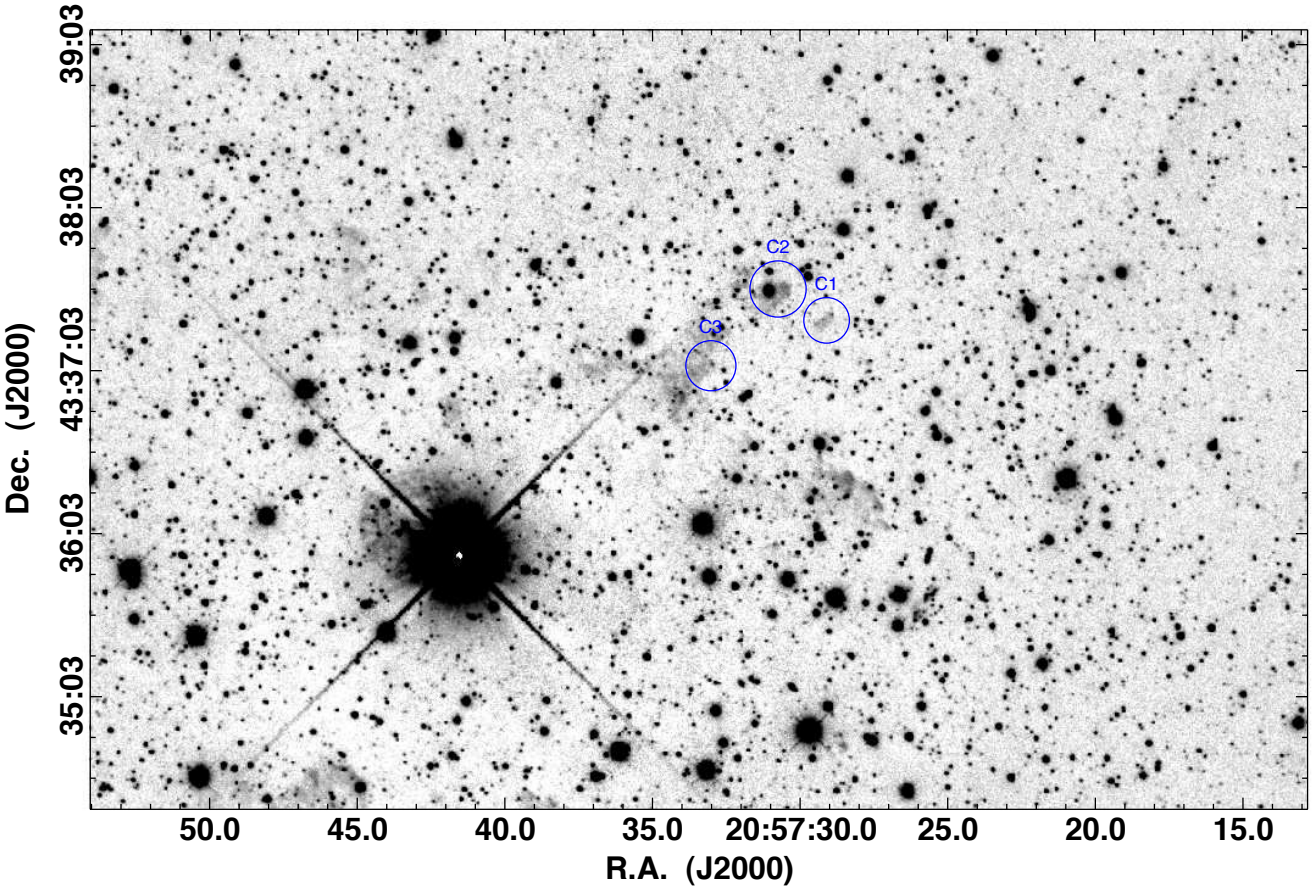

Fig. 22.— 2.12 μm image showing several cometary clouds (C1 through C3) southeast of the Gulf of Mexico.

Table 1. MHOs and Reflection Nebulae in the Pelican

α J2000	δ J2000	#[1]	MHO[2]	Comments
20 50 03.1	+44 34 58	4	3400	W4 west-end of east-west flow
20 50 13.4	+44 34 51	5	3400	W3
20 50 14.8	+44 34 51	6	3400	W2
20 50 16.1	+44 34 50		3400	W1 jet at PA $\sim$ 275deg
20 50 17.9	+44 34 46	7	3400	E1 jet at PA $\sim$ 95deg
20 50 20.0	+44 34 40		3400	E2
20 50 21.3	+44 34 42	8	3400	E3
20 50 31.7	+44 35 25	9	3400	E4 east end of east-west flow
20 50 15.1	+44 32 20	10		bow from MHO 3401 or fluorescent edge?
20 50 14.9	+44 33 25	11	3400	S5 south-end of pair of north-south flow
20 50 15.8	+44 33 51		3400	S4 dim complex of knots
20 50 15.2	+44 34 15	12	3400	S3 bright knot
20 50 15.7	+44 34 32		3400	S2 bright knot
20 50 16.1	+44 34 38	13	3400	S1 jet at PA $\sim$ 185deg
20 50 18.1	+44 35 08	14	3400	N1
20 50 18.6	+44 35 15		3400	N2
20 50 19.0	+44 35 24		3400	N3
20 50 19.4	+44 35 34	15	3400	N4 north-end of 4 knot chain
20 50 20.6	+44 36 26	16	3400	N5 north-end of north-south flow?
20 49 48.6	+44 34 26	1	3401	W2 Flow from isolated clump
20 49 50.7	+44 34 04	2	3401	W1
20 49 54.3	+44 33 39	3	3401	E1
20 50 46.4	+44 33 19	17	3402	W3 Cluster of knots; 2 flows?
20 50 47.3	+44 33 29		3402	W2
20 50 48.5	+44 33 38	18	3402	W1
20 50 48.8	+44 33 31	19	3402	E1
20 50 49.8	+44 33 33		3402	E2
20 50 50.0	+44 33 36		3402	E3
20 50 50.4	+44 33 38		3402	E4
20 50 50.3	+44 33 44	20	3402	E5

Table 1—Continued

α J2000	δ J2000	#[1]	MHO[2]	Comments
20 50 37.7	+44 21 38	21	3403	HH 567
20 50 38.7	+44 21 38	22	3403	HH 569 bow
20 50 28.2	+44 23 56	23	3404	part of SE-NW chain
20 50 31.5	+44 23 19	24	3404	”
20 50 33.6	+44 22 55	25	3404	”
20 50 34.5	+44 22 31	26	3404	”
20 51 18.9	+44 25 54	-	3405	HH 555 north
20 51 18.5	+44 25 19	-	3405	HH 555 south
20 50 42.8	+44 21 42	27	3406	south of IRAS 2489+4410
20 50 42.9	+44 22 10	28	3406	north of IRAS 2489+4410
20 50 42.2	+44 22 14	29	3406	”
20 50 42.0	+44 22 33	30	3407	”
20 50 38.7	+44 22 54	31	3407	northwest of IRAS 2489+4410
20 50 34.9	+44 23 24	32	3407	
20 50 16.9	+44 22 59	33	3408	fainter of two knots
20 50 23.0	+44 23 06	34	3408	brighter knot
20 50 26.3	+44 25 39	35	3409	compact knot west of IRS 6
20 50 42.1	+44 25 57	35	3409	compact knot northeast of IRS 6
20 50 44.8	+44 20 40	36	3410	north of IRAS 20489+4406
20 50 44.1	+44 19 50	37	3410	”
20 50 41.7	+44 18 40	38	3410	”
20 50 39.9	+44 17 12	39	3410	south of IRAS 20489+4406
20 50 39.4	+44 15 43	-	3410	HH 565
20 50 38.9	+44 13 58	-	3410	HH 564
20 50 32.9	+44 12 50	-	3410	HH 563
20 50 43.3	+44 16 58	40	3411	east of HH 3410
20 49 29.0	+44 17 17	41	3412	compact bow at west edge
20 49 30.2	+44 17 01			R1
20 50 08.4	+44 26 59			R2
20 50 09.7	+44 26 53			R3

Table 1—Continued

α J2000	δ J2000	#[1]	MHO[2]	Comments
20 50 42.8	+44 21 56			R4
20 50 46.8	+44 33 24			R5
20 49 52.1	+44 33 48			Pelican IRS 1
20 49 51.8	+44 33 55			Pelican IRS 2; source of MHO 3401
20 50 16.6	+44 34 49			Pelican IRS 3; source of MHO 3400, IRAS IRAS 20485+4423
20 50 46.8	+44 33 25			Pelican IRS4; MHO 3402
20 50 09.2	+44 26 51			Pelican IRS5a
20 50 07.5	+44 26 59			Pelican IRS5b
20 50 32.3	+44 25 06			Pelican IRS6
20 50 36.8	+44 21 40			Pelican IRS7a
20 50 35.8	+44 21 50			Pelican IRS7b
20 50 34.8	+44 22 23			Pelican IRS7c
20 50 42.8	+44 21 55			Pelican IRS8
20 50 50.1	+44 24 39			Pelican IRS 9
20 50 27.4	+44 19 53			Pelican IRS 10
20 50 40.8	+44 18 07			Pelican IRS 11
20 50 27.8	+44 32 06			Pelican IRS 12
20 50 27.5	+44 23 28			Pelican IRS 13
20 50 36.7	+44 23 09			Pelican IRS 14
20 50 37.9	+44 18 45			Pelican IRS 15
20 50 53.3	+44 24 49			Pelican IRS 16
20 50 49.8	+44 23 40			Pelican IRS 17
20 50 45.7	+44 24 46			Pelican IRS 18
20 50 53.7	+44 15 57			Pelican IRS 19
20 51 19.3	+44 25 38			Pelican IRS 20
20 49 52.8	+44 15 38			Pelican IRS 21

Note. — **[1]**: The numbers refer to those marked in Figure 5. **[2]**: MHO (Molecular Hydrogen Object) numbers refer to the catalog entries in the MHO catalog (http://www.astro.ljmu.ac.uk/MHCat/). **[3]**: Reflection nebulae are indicated by a letter 'R' followed by a number which corresponds to the entries in the Figures.

Table 2. MHOs and Reflection Nebulae in the Atlantic Region

α J2000	δ J2000	#	MHO	Comments
20 53 31.9	+44 30 22	1	MHO 3413	[FeII] and H_2
20 53 29.7	+44 29 38	2	”	[FeII] only
20 53 28.9	+44 29 25	3	”	[FeII] only
20 53 25.8	+44 28 31	4	”	[FeII] only
20 53 37.5	+44 31 26	5	”	counterjet [FeII] only
20 53 41.7	+44 31 59	6	”	[FeII] only; very faint
20 53 30.9	+44 30 03		IR source	Source of MHO 3413 & 3415 ?
20 53 38.7	+44 34 09	7	MHO 3414	H_2 only; north of IRAS20518+4420
20 53 36.1	+44 34 39	8	”	H_2
20 53 36.0	+44 34 58	9	”	H_2
20 53 32.5	+44 35 35	10	”	H_2
20 53 54.2	+44 38 16	11	MHO 3415	H_2 knot
20 53 09.6	+44 32 57	12	MHO 3416	[FeII] and H_2; west of IRAS20518+4420
20 53 08.3	+44 33 07	13	”	[FeII] and H_2

Note. — [**1**]: Labeling same as in Table 1.

Table 3. MHOs, Reflection Nebulae, and IR Sources in the Gulf-of-Mexico Region

α J2000	δ J2000	#[1]	MHO[2]	Comments
	Gulf	SW2		
20:56:41.6	43:48:41	1	3417	HH 953 large bow, north end
20:56:46.4	43:45:31	2	”	
20:56:49.2	43:44:54	3	”	
20:56:54.3	43:42:21	4	”	
20:56:57.2	43:40:37	5	3417	HH 954 large bow, south end
20:56:56.6	43:40:05	6	”	faint knot
20:56:59.7	43:40:17	7	”	faint knot
20:56:49.0	43:45:13	IRS 1		S_{70} = 6.1 Jy
20:56:51.1	43:44:06	IRS 2		S_{70} = 2.9 Jy
20:56:47.3	43:43:08	8	3418	west of 3417
20:56:50.7	43:42:15	9	”	
20:56:47.7	43:46:43	IRS 3		S_{70} = 3.4 Jy
20:56:49.3	43:47:29	10	3419	bright bow, east of 3417
20:56:48.9	43:44:06	IRS 4		S_{70} = 1.9 Jy
20:56:52.1	43:47:38	IRS 5		S_{70} = 1.9 Jy
20:56:53.5	43:38:22	11	3420	isolated compact bow
20:57:00.7	43:34:38	12	3421	irregular bright H_2 knots ; HH 1087
20:57:01.4	43:34:59	13	”	near R7
20:57:01.8	43:34:47	14	”	
20:57:05.1	43:34:28	IRS 6		S_{70} = 0.4 Jy
20:57:09.1	43:36:07	15	3422	southeast of R5
20:57:13.2	43:36:27	16	”	
20:57:07.1	43:37:04	IRS 7		S_{70} = 2.7 Jy
20:57:11.8	43:39:42	17	3423	east of knot 5
20:57:22.3	43:40:05	18	”	
20:57:05.7	43:43:06	19	3424	east of MHO 3418
20:57:09.8	43:42:45	20	”	
20:57:13.2	43:42:32	21	”	
20:57:00.8	43:44:43	22	3425	south facing bow

Table 3—Continued

α J2000	δ J2000	#[1]	MHO[2]	Comments
	Gulf	SW1		
20:57:18.5	43:48:42	23	3426	west
20:57:20.7	43:48:50	24	”	west
20:57:22.4	43:49:00	25	”	east
20:57:23.0	43:49:01	26	”	east
20:57:23.8	43:49:02	27	”	east
20:57:20.7	43:48:51	IRS 8	”	S_{70} = 0.4 Jy
20:57:23.9	43:47:35	28	3427	west
20:57:27.5	43:48:00	29	”	
20:57:32.0	43:47:53	30	”	
20:57:33.4	43:47:52	31	”	
20:57:29.9	43:47:22	IRS 9		S_{70} = 0.6 Jy
20:57:37.1	43:48:03	IRS 10		S_{70} = 0.1 Jy
20:57:38.7	43:48:09	32	3427	east
20:57:40.8	43:48:17	33	”	
20:57:41.9	43:48:20	34	”	
20:57:42.3	43:48:20	35	”	
20:57:42.3	43:48:09	36	”	
20:57:43.3	43:48:16	37	”	
20:57:44.5	43:48:23	38	”	
20:57:45.8	43:48:18	39	”	
20:57:52.5	43:48:35	40	”	
	Gulf	core		
20:57:55.4	43:50:16	41	3428	HH 639
20:57:58.8	43:49:33	42	”	
20:57:51.4	43:51:40	43	3429	HH 638
20:57:44.3	43:51:29	44	3430	HH 636
20:57:45.9	43:52:50	45	”	
20:57:45.5	43:53:22	IRS 11		
20:57:45.2	43:53:40	46	3431	HH 637

Table 3—Continued

α J2000	δ J2000	#[1]	MHO[2]	Comments
20:57:44.0	43:53:40	47	”	
20:57:45.3	43:53:55	48	”	
20:57:43.1	43:53:22	49	3432	HH 640 counterflow?
20:57:46.6	43:53:23	50	3434	HH 640
20:57:47.4	43:53:25	IRS 12		
20:57:35.2	43:55:25	51	3433	
20:57:33.8	43:55:51	52	”	HH 1088
20:57:29.3	43:56:45	53	”	
20:57:49.4	43:53:29	54	3435	HH 640
20:57:49.8	43:53:28	55	”	between 54 & 57
20:57:50.5	43:53:27	56	”	between 54 & 57
20:57:50.8	43:53:25	57	”	
20:57:51.6	43:53:23	58	”	
20:57:52.4	43:53:20	59	”	
20:57:53.2	43:53:16	60	”	
20:57:53.8	43:53:01	61	”	continuation of MHO 3435 ?
20:57:54.0	43:52:58	62	”	
20:57:56.5	43:52:50	63		HH 643
20:57:58.9	43:52:40	64		
20:57:59.5	43:52:45	65		
20:58:04.3	43:52:10	74		
20:57:51.8	43:53:10	66	3436	
20:57:52.1	43:53:13	67		
20:57:54.1	43:53:40	68		
20:57:54.7	43:53:51	69		
20:57:55.4	43:54:01	70	HH 642	
20:57:57.0	43:54:50	71		
20:57:52.2	43:54:04	72	3437	HH 641 R15
20:57:52.1	43:53:50	IRS 13		
20:57:57.7	43:53:22	73	3438	

Table 3—Continued

α J2000	δ J2000	#[1]	MHO[2]	Comments
20:58:24.3	43:50:43	75	3439	HH 1089
20:58:15.2	43:52:01	76	”	
20:58:13.0	43:52:22	77	”	
20:58:12.0	43:52:30	78	”	
20:58:10.8	43:52:27	79		HH 651
20:58:04.7	43:52:33	80	3440	HH 648
20:58:06.7	43:52:46	81	”	
20:58:09.0	43:53:02	82	”	
20:58:08.5	43:52:47	83	3441	HH 649
20:58:11.8	43:53:02	84	”	
20:58:12.5	43:53:02	84e	”	
20:58:08.9	43:53:13	82n	3442	filament north of 82
20:58:06.1	43:53:34	85	3443	
20:58:05.3	43:53:57	86	”	
20:58:03.8	43:54:32	87	”	
20:58:02.3	43:54:09	88	”	HH 647
20:57:59.7	43:53:55	IRS 14		
20:58:06.0	43:53:49	IRS 15		
20:58:09.3	43:54:54	89	3444	
20:58:09.9	43:54:37	90	”	
20:58:11.6	43:53:45	91	3445	
20:58:13.0	43:53:57	92	”	
20:58:13.7	43:53:08	95		HH 650
20:58:15.3	43:53:52	96	3446	HH 657
20:58:18.4	43:53:11	97	”	
20:58:19.9	43:53:00	98	”	
20:58:21.7	43:52:37	99	”	
20:58:21.4	43:52:25	100	”	
20:58:19.0	43:52:36	101	”	
20:58:18.2	43:54:39	102	3447	

Table 3—Continued

α J2000	δ J2000	#[1]	MHO[2]	Comments
20:58:18.8	43:54:55	103	”	
20:58:23.4	43:54:30	104	3448	HH 658
20:58:26.0	43:53:16	105	3449	
20:58:26.9	43:53:05	106	”	
20:58:16.8	43:57:52	108	3450	
20:58:20.7	43:57:39	109	”	
20:58:23.5	43:57:22	110	”	
20:58:21.5	43:57:35	IRS 16		
20:58:28.0	43:56:47	111	3451	
20:58:29.0	43:56:24	112	”	
20:58:28.7	43:56:13	113	”	
	Reflection	Nebulae		
20:56:50.7	43:44:06	R1		IRS 2 MHO 3417
20:56:48.8	43:46:40	R2		IRS 4 MHO 3419
20:56:46.0	43:43:20	R3		MHO 3418
20:56:17.0	43:38:51	R4		
20:57:06.9	43:36:50	R5		IRS 7 MHO 3422
20:57:08.9	43:37:40	R6		
20:57:05.0	43:34:18	R7		IRS 6 MHO 3421
20:57:10.1	43:32:00	R8		
20:57:29.7	43:47:22	R9		IRS 9 Gulf Core SW1
20:57:39.7	43:52:03	R10		west-end of Gulf core W
20:57:47.7	43:52:39	R11		
20:57:49.4	43:52:37	R12		MHO 3429
20:57:45.5	43:53:22	R13		IRS 11
20:57:47.0	43:53:24	R14		IRS 12
20:57:51.9	43:53:48	R15		IRS 13
20:57:55.2	43:53:35	R16		
20:57:52.9	43:53:28	R17		
20:57:49.7	43:53:22	R18		

Table 3—Continued

α J2000	δ J2000	#[1]	MHO[2]	Comments
20:58:18.2	43:53:28	R19		Herbig cluster
20:58:20.6	43:56:44	R20		south of R21
20:58:21.5	43:57:35	R21		MHO 3450
	Cometary	Clouds		
20:57:29.0	43:37:21	C1		
20:57:30.7	43:37:33	C2		
20:57:33.0	43:37:05	C3		
20:57:58.5	43:41:14	C4		
20:58:02.7	43:40:50	C5		
20:58:08.5	43:40:30	C6		
20:58:14.1	43:39:27	C7		
20:58:05.0	43:42:25	C8		
20:58:18.6	43:39:19	C9		
20:58:19.0	43:40:01	C10		
20:58:28.8	43:43:26	C11		
20:58:39.8	43:30:46	C12		
20:58:39.9	43:31:12	C13		
20:58:40.4	43:32:26	C14		
20:58:42.2	43:31:38	C15		
20:58:43.4	43:32:12	C16		
20:58:43.5	43:31:14	C17		
20:58:51.4	43:36:14	C18		

Note. — **[1]:** Numbers as in Table 1. Numbers following a letter 'C' refer to cometary clouds whose edges are lit up with fluorescent H_2 emission. Numbers following a letter 'R' refer to infrared reflection nebula detected in the K_s images. Numbers preceded by 'IRS' refer to infrared sources in the Gulf region. **[2]:** MHO numbers.

Table 4. Properties of Bolocam Clumps and Cores

Object	α J2000	δ J2000	S_ν (Jy)	M ($M_\odot$)	Comments
Pelican MHO 3401	20 49 50.6	+44 34 11	1.2	9	r = 77″ by 83″ oval
Pelican MHO 3400	20 50 15.3	+44 34 46	1.2	9	r = 65″ by 55″ oval
Pelican MHO 3402	20 50 40.9	+44 33 51	1.6	12	r = 58″ by 111″ oval
Pelican 4	20 50 30.1	+44 25 11	1.4	10	r = 74″ by 60″ oval
Pelican 5	20 50 49.0	+44 25 07	2.2	16	r = 74″ by 60″ oval
Pelican 6	20 50 33.2	+44 22 44	1.5	11	r = 56 ″ by 49″ oval
Pelican 7	20 50 44.6	+44 22 30	1.9	14	r = 64″ by 92″ oval
Pelican 8	20 50 40.7	+44 18 12	2.6	19	r = 36″ by 46″ oval
Pelican 9	20 50 28.7	+44 19 05	7.8	56	contains 8; 209″ by 103″ oval
Pelican total	20 50 06.1	+44 30 59	17.9	129	550″ by 1030″ oval
Atlantic main	20 53 34.8	+44 32 24	30.1	216	r = 257″
Atlantic 1	20 54 05.3	+44 23 36	2.0	14	155″ by 73″ oval
Atlantic 2	20 54 32.1	+44 13 45	2.8	20	160″ by 76″ oval
Gulf core E	20 58 13.0	+43 53 00	4.4	32	r = 95″
Gulf core W	20 57 49.1	+43 53 00	8.9	64	r = 162″ by 95″ oval
Gulf SW1	20 57 36.0	+43 47 56	4.2	30	r = 82″
Gulf SW2 main	20 56 45.7	+43 43 41	66.3	477	r = 345″ by 159″ oval
Gulf SW2 SE	20 57 09.5	+43 40:39	16.6	119	r = 292″ by 130″ oval
Gulf SW2 S	20 57 06.3	+43 32 31	3.6	26	r = 235″ by 150″ oval
Gulf total	20 57 22.0	+43 42 24	108.0	776	r = 1105″ by 548″ oval

Note. — [**1**]: Masses are computed from the area-integrated flux S_ν in units of Janskys using $M = 14.26(e^{(13.01/T_K)} - 1)D^2(kpc)S_\nu(Jy)$ $M_\odot$ where $D(kpc)$ is the distance in kpc. For an adopted distance $D(kpc) = 0.55$ kpc and $T_K = 20$ Kelvin, $M = 7.19S_\nu(Jy)$ $M_\odot$. [**2**]: The entries for Pelican total and Gulf total are based on the integrated fluxes measured in the large ovals and not derived by summing the masses of the individual clumps.